Coupling Stokes-Darcy flow with transport

Danail Vassilev[*] Ivan Yotov[†]

August 4, 2008

Abstract

A mathematical and numerical model describing chemical transport in a Stokes-Darcy flow system is discussed. The flow equations are solved through domain decomposition using classical finite element methods in the Stokes region and mixed finite element methods in the Darcy region. The local discontinuous Galerkin (LDG) method is used to solve the transport equation. Models dealing with coupling between Stokes and Darcy equations have been extensively discussed in the literature. This paper focuses on the approximation of the transport equation. Stability of the LDG scheme is analyzed and an *a priori* error estimate is proved. Several numerical examples verifying the theory and illustrating the capabilities of the method are presented.

Keywords: Stokes-Darcy flow, coupled flow and transport, error estimates, local discontinuous Galerkin.

1 Introduction

Coupling the Stokes and Darcy equation has become a very active area of research because of its potential for practical applications. Such models can be used to describe physiological phenomena like the blood motion in the vessels, hydrological systems in which surface water percolates through rocks and sand, and various industrial processes involving filtration. One serious problem today is surface water and groundwater contamination resulting from leaky underground storage tanks, chemical spills, and various human activities. A model coupling the Stokes-Darcy equations with a transport equation can be used to study the spread of pollution released in the water and assess the danger.

There are number of stable and convergent numerical methods developed for the coupled Stokes-Darcy flow system, see e.g., [25, 21, 26, 29, 23]. We will concentrate on the

[*]Department of Mathematics, University of Pittsburgh, 301 Thackeray Hall, Pittsburgh, Pennsylvania 15260, USA; `dhv1@pitt.edu`.

[†]Department of Mathematics, University of Pittsburgh, 301 Thackeray Hall, Pittsburgh, Pennsylvania 15260, USA; `yotov@math.pitt.edu`.

methods developed in [25, 29]. Both methods utilize a mixed finite element (MFE) method in the porous media domain, which computes the velocity directly and with high accuracy. Furthermore the MFE method incorporates the Neumann boundary condition (2.6) into the velocity approximating space, which allows for a more accurate treatment of the inflow boundary condition (2.13) in the transport problem, see (3.4). Also, MFE methods provide locally mass conservative velocities, a property critical for the transport problem in order to avoid creating artificial mass sources and sinks. The method developed in [29] is especially suited for coupling with transport, since there a discontinuous Galerkin (DG) approximation is used for the Stokes equation, giving locally mass conservative velocities in the Stokes region as well.

The focus of this paper is the coupling of the Stokes-Darcy flow system with an advection-diffusion equation that models transport of a chemical. For the numerical approximation of the transport problem we employ the local discontinuous Galerkin (LDG) method [15, 13], which conserves mass locally and approximates sharp fronts accurately. The method can be defined on general grids and allows one to vary the degree of the approximating polynomial space from element to element. The LDG method can be thought of as a discontinuous mixed finite element method, since it approximates both the concentration and the diffusive flux. Primal DG discretizations of advection-diffusion equations have also been studied [32] and could be applied for our problem. For the sake of space we limit our presentation to LDG discretizations. Couplings of Darcy flow with DG approximations for transport have been studied in [31, 20].

In this paper we develop stability and convergence analysis for the concentration and the diffusive flux in the transport equation. The numerical error is a combination of the LDG discretization error and the error from the discretization of the Stokes-Darcy velocity. The former is shown to be of the order $O(h^k)$, where k is the polynomial degree in the LDG approximating space. This is similar to existing bounds in the literature for stand-alone LDG discretizations [15, 13, 10]. The error terms coming from the Stokes-Darcy flow discretization are of optimal order, similar to the bounds obtained in [25, 29]. This is an improvement of $O(h)$ from the result in [18], where the Darcy velocity discretization error is incorporated into the error analysis of the transport equation. We also extend previous LDG transport analysis [15, 18, 10, 13] to non-divergence free velocity.

The rest of the paper is organized as follows. In Section 2 we present the model flow-transport problem. The Stokes-Darcy flow discretization and the LDG transport discretization are given in Sections 3 and 4, respectively. Section 5 is devoted to the stability of the LDG scheme. The error analysis of the LDG method is presented in Section 6. The paper ends with numerical experiments in Section 7.

2 Model problem

In our model we consider a fluid region $\Omega_1 \subset \mathbb{R}^d$, $d = 2, 3$, in which the flow is governed by the Stokes equations (2.1)–(2.3) and a porous medium $\Omega_2 \subset \mathbb{R}^d$ in which Darcy's law

(2.4)–(2.6) holds. The two regions are separated by an interface Γ_{12} through which the fluid can flow in both directions. Let $\mathbf{n}_i$ be the outward unit normal vector to $\partial\Omega_i$, $i = 1, 2$, let $\boldsymbol{\tau}_j$, $j = 1, d-1$, be an orthonormal system of tangential vectors on Γ_{12}, and let $\Gamma_i := \partial\Omega_i \setminus \Gamma_{12}$. Let $\mathbf{u}_i : \Omega_i \to \mathbb{R}^d$ and $p_i : \Omega_i \to \mathbb{R}$ denote, respectively, the velocity and the pressure in Ω_i. Let $\mathbf{De}(\mathbf{u}_1)$ and $\mathbf{T}(\mathbf{u}_1, p_1)$ and denote, respectively, the deformation rate tensor and the stress tensor:

$$\mathbf{De}(\mathbf{u}_1) = \frac{1}{2}(\nabla\mathbf{u}_1 + \nabla\mathbf{u}_1^T), \quad \mathbf{T}(\mathbf{u}_1, p_1) = -p_1\mathbf{I} + 2\mu\mathbf{De}(\mathbf{u}_1),$$

where μ is the fluid viscosity. Let $\mathbf{f}_1 \in (L^2(\Omega_1))^d$ be body force in Ω_1 and let $\mathbf{g}_1 \in (H^{1/2}(\Gamma_1))^d$ be boundary velocity data. In Ω_2, $\mathbf{K}$ is a symmetric and positive definite rock permeability tensor with components bounded from above, $\mathbf{f}_2 \in (L^2(\Omega_2))^d$ represents the gravity force, $q_2 \in L^2(\Omega_2)$ is a source (sink) function satisfying the solvability condition (2.7), and $g_2 \in L^2(\Omega_2)$ is boundary normal velocity data. In addition we also assume that on Γ_{12} the interface conditions (2.8)–(2.10) are satisfied. The flow model is

$$\begin{aligned} -\nabla\cdot\mathbf{T} \equiv -2\mu\nabla\cdot\mathbf{De}(\mathbf{u}_1) + \nabla p_1 &= \mathbf{f}_1 \quad \text{in } \Omega_1, && (2.1)\\ \nabla\cdot\mathbf{u}_1 &= 0 \quad \text{in } \Omega_1, && (2.2)\\ \mathbf{u}_1 &= \mathbf{g}_1 \quad \text{on } \Gamma_1, && (2.3) \end{aligned}$$

$$\begin{aligned} \mu\mathbf{K}^{-1}\mathbf{u}_2 + \nabla p_2 &= \mathbf{f}_2 \quad \text{in } \Omega_2, && (2.4)\\ \nabla\cdot\mathbf{u}_2 &= q_2 \quad \text{in } \Omega_2, && (2.5)\\ \mathbf{u}_2\cdot\mathbf{n}_2 &= g_2 \quad \text{on } \Gamma_2, && (2.6) \end{aligned}$$

$$\int_{\Omega_2} q_2\, d\mathbf{x} = \int_{\Gamma_1} \mathbf{g}_1\cdot\mathbf{n}_1\, d\sigma + \int_{\Gamma_2} g_2\, d\sigma, \tag{2.7}$$

$$\begin{aligned} \mathbf{u}_1\cdot\mathbf{n}_1 + \mathbf{u}_2\cdot\mathbf{n}_2 &= 0 \quad \text{on } \Gamma_{12}, && (2.8)\\ -\mathbf{n}_1\cdot\mathbf{T}\cdot\mathbf{n}_1 \equiv p_1 - 2\mu\mathbf{n}_1\cdot\mathbf{De}(\mathbf{u}_1)\cdot\mathbf{n}_1 &= p_2 \quad \text{on } \Gamma_{12}, && (2.9)\\ -\frac{\sqrt{K_j}}{\mu\alpha}\mathbf{n}_1\cdot\mathbf{T}\cdot\boldsymbol{\tau}_j \equiv -\frac{\sqrt{K_j}}{\alpha}2\mathbf{n}_1\cdot\mathbf{De}(\mathbf{u}_1)\cdot\boldsymbol{\tau}_j &= \mathbf{u}_1\cdot\boldsymbol{\tau}_j,\ j = 1, d-1, \text{ on } \Gamma_{12} && (2.10) \end{aligned}$$

Conditions (2.8) and (2.9) impose continuity of flux and normal stress, respectively. Condition (2.10) is known as the Beavers-Joseph-Saffman law [5, 30], where $K_j = \boldsymbol{\tau}_j\cdot\mathbf{K}\cdot\boldsymbol{\tau}_j$ and $\alpha > 0$ is an experimentally determined dimensionless constant.

The Stokes-Darcy flow system is coupled with the transport equation on $\Omega = \Omega_1 \cup \Omega_2$:

$$\phi c_t + \nabla\cdot(c\mathbf{u} - \mathbf{D}\nabla c) = \phi s \ , \ \forall(\mathbf{x}, t) \in \Omega \times (0, T), \tag{2.11}$$

where $c(\mathbf{x}, t)$ is the concentration of some chemical component, $0 < \phi_* \le \phi(\mathbf{x}) \le \phi^*$ is the porosity of the medium in Ω_2 (it is set to 1 in Ω_1), $\mathbf{D}(\mathbf{x}, t)$ is the diffusion/dispersion tensor assumed to be symmetric and positive definite, $s(\mathbf{x}, t)$ is a source term, and $\mathbf{u}$ is the velocity field defined by $\mathbf{u}|_{\Omega_i} = \mathbf{u}_i$, $i = 1, 2$. The model is completed by the initial condition

$$c(\mathbf{x}, 0) = c^0(\mathbf{x}) \ , \ \forall \mathbf{x} \in \Omega \tag{2.12}$$

and the boundary conditions

$$(c\mathbf{u} - \mathbf{D}\nabla c) \cdot \mathbf{n} \;=\; (c_{in}\mathbf{u}) \cdot \mathbf{n} \ \text{ on } \ \Gamma_{in}, \tag{2.13}$$

$$(\mathbf{D}\nabla c) \cdot \mathbf{n} \;=\; 0 \ \text{ on } \ \Gamma_{out}. \tag{2.14}$$

Here $\Gamma_{in} := \{\mathbf{x} \in \partial\Omega : \mathbf{u} \cdot \mathbf{n} < 0\}$, $\Gamma_{out} := \{\mathbf{x} \in \partial\Omega : \mathbf{u} \cdot \mathbf{n} \geq 0\}$, and $\mathbf{n}$ is the unit outward normal vector to $\partial\Omega$. We will also use the notation $\Gamma = \partial\Omega$.

Throughout the paper K will denote a generic constant independent of the discretization parameters h_1, h_2, and h. We will use the following standard notation. For a domain $G \subset \mathbb{R}^d$, the $L^2(G)$ inner product and norm for scalar and vector valued functions are denoted $(\cdot, \cdot)_G$ and $\| \cdot \|_G$, respectively. The norms and seminorms of the Sobolev spaces $W^{k,p}(G)$, $k \in \mathbb{R}$, $p > 0$ are denoted by $\| \cdot \|_{k,p,G}$ and $| \cdot |_{k,p,G}$, respectively. The norms and seminorms of the Hilbert spaces $H^k(G)$ are denoted by $\| \cdot \|_{k,G}$ and $| \cdot |_{k,G}$, respectively. We omit G in the subscript if $G = \Omega$. For a section of the domain or element boundary $S \subset \mathbb{R}^{d-1}$ we write $\langle \cdot, \cdot \rangle_S$ and $\| \cdot \|_S$ for the $L^2(S)$ inner product (or duality pairing) and norm, respectively.

3 Stokes-Darcy flow discretization

Let $\mathcal{T}_{h,i}$ be a a shape-regular affine finite element partition of Ω_i [12] with a maximum element diameter h_i, $i = 1, 2$. We allow for the traces of the grids on Γ_{12} to be non-matching and assume that no point of the interface boundary $\partial\Gamma_{12}$ belongs to the interior of a face of an element of $\mathcal{T}_{h,2}$. We consider two possibilities for the flow discretization on Ω_1.

The first choice, which follows [25], is to let $\mathbf{X}_{h,1} \times M_{h,1}$ be any of the known conforming and stable Stokes finite element spaces, for example the MINI elements [4], the Taylor–Hood elements [33], or the conforming Crouzeix–Raviart elements [17]. We assume that $\mathbf{X}_{h,1}$ and $M_{h,1}$ include at least polynomials of degree k_1 and $k_1 - 1$ respectively ($k_1 \geq 1$).

The second choice, following [29], is to let $\mathbf{X}_{h,1} \times M_{h,1}$ be a pair of discontinuous piecewise polynomial spaces such that on each element of $\mathcal{T}_{h,1}$ the space $\mathbf{X}_{h,1}$ contains vectors with components polynomials of degree k_1 and the space $M_{h,1}$ contains polynomials of degree $k_1 - 1$. In this second case we assume that $\Omega \subset \mathbb{R}^2$.

In both cases, for the discretization of the Darcy model in Ω_2, we take $\mathbf{X}_{h,2} \times M_{h,2}$ to be any of the standard mixed finite element spaces, the RT spaces [28, 27], the BDM spaces [8], the BDFM spaces [7], the BDDF spaces [6], or the CD spaces [11]. We assume that $\mathbf{X}^{h,1}$ and $M^{h,2}$ contain at least polynomials of degree k_2 and l_2, respectively.

The analysis in both [25] and [29] allows for non-matching grids across Γ_{12}, even though this is not explicitly stated in [25].

Let

$$\mathbf{X}_h = \mathbf{X}_{h,1} \times \mathbf{X}_{h,2}, \quad M_h = \{w = (w_1, w_2) \in M_{h,1} \times M_{h,2} : (w_1, 1)_{\Omega_1} + (w_2, 1)_{\Omega_2} = 0\}$$

and

$$\mathbf{X}_{h,0} = \{\mathbf{v} = (\mathbf{v}_1, \mathbf{v}_2) \in \mathbf{X}_h : \langle \mathbf{v}_1 \cdot \mathbf{n}_1 + \mathbf{v}_2 \cdot \mathbf{n}_2, \mu \rangle_{\Gamma_{12}} = 0 \quad \forall \mu \in \mathbf{X}_{h,2} \cdot \mathbf{n}_2\}.$$

To save space we will only present the method based on conforming Stokes elements [25]. We refer the reader to [29] for details on the discontinuous Stokes discretization for the coupled Stokes-Darcy problem. Let

$$\mathbf{X}_{h,1}^0 = \{\mathbf{v} \in \mathbf{X}_{h,1} : \mathbf{v} = 0 \text{ on } \Gamma_1\},$$

$$\mathbf{X}_{h,2}^0 = \{\mathbf{v} \in \mathbf{X}_{h,2} : \mathbf{v} \cdot \mathbf{n} = 0 \text{ on } \Gamma_2\},$$

$$\mathbf{X}_h^0 = \mathbf{X}_{h,1}^0 \times \mathbf{X}_{h,2}^0, \quad \text{and} \quad \mathbf{X}_{h,0}^0 = \mathbf{X}_h^0 \cap \mathbf{X}_{h,0}.$$

Let $\mathbf{u}_g \in H(\mathrm{div}; \Omega)$ be such that $\mathbf{u}_g|_{\Omega_1} \in H^1(\Omega_1)$, $\mathbf{u}_g = \mathbf{g}_1$ on Γ_1 and $\mathbf{u}_g \cdot \mathbf{n}_2 = g_2$ on Γ_2. Let $\mathbf{U}_g \in \mathbf{X}_{h,0}$ be a suitable approximation to u_g. The numerical scheme for the coupled Stokes-Darcy flow problem is: find $\mathbf{U} \in \mathbf{X}_{h,0}^0 + \mathbf{U}_g$ and $P \in M_h$ such that

$$\begin{aligned} a(\mathbf{U}, \mathbf{v}) + b(\mathbf{v}, P) &= (\mathbf{f}, \mathbf{v}), \quad \forall\, \mathbf{v} \in \mathbf{X}_{h,0}^0, && (3.1) \\ b(\mathbf{U}, w) &= -(q_2, w)_{\Omega_2}, \quad \forall\, w \in M_h, && (3.2) \end{aligned}$$

where $a(\cdot, \cdot) = a_1(\cdot, \cdot) + a_2(\cdot, \cdot)$, $b(\cdot, \cdot) = b_1(\cdot, \cdot) + b_2(\cdot, \cdot)$,

$$a_1(\mathbf{u}_1, \mathbf{v}_1) = (2\mu \mathbf{D}(\mathbf{u}_1), \mathbf{D}(\mathbf{v}_1))_{\Omega_1} + \sum_{j=1}^{d-1} \left\langle \frac{\mu\alpha}{\sqrt{K_j}} \mathbf{u}_1 \cdot \boldsymbol{\tau}_j, \mathbf{v}_1 \cdot \boldsymbol{\tau}_j \right\rangle_{\Gamma_{12}},$$

$$a_2(\mathbf{u}_2, \mathbf{v}_2) = (\mu \mathbf{K}^{-1} \mathbf{u}_2, \mathbf{v}_2)_{\Omega_2}, \quad \text{and} \quad b_i(\mathbf{v}_i, w_i) = -(\nabla \cdot \mathbf{v}_i, w_i)_{\Omega_i}, \ i = 1, 2.$$

We take $\mathbf{U}_g$ to be any function in $\mathbf{X}_{h,0}$ such that $\mathbf{U}_g = Q_{h,1}\mathbf{g}_1$ on Γ_1 and $\mathbf{U}_g \cdot \mathbf{n}_2 = Q_{h,2} g_2$ on Γ_2, where $Q_{h,1}$ is the $L^2(\Gamma_1)$-projection onto $\mathbf{X}_{h,1}|_{\Gamma_1}$ and $Q_{h,2}$ is the $L^2(\Gamma_2)$-projection onto $\mathbf{X}_{h,2} \cdot \mathbf{n}_2|_{\Gamma_2}$. The computed flow solution is independent of the choice of $\mathbf{U}_g$ and depends only on $Q_{h,1}\mathbf{g}_1$ and $Q_{h,2} g_2$. For the homogeneous boundary conditions case, it was shown in [25] that the above method has a unique solution satisfying

$$\|\mathbf{u} - \mathbf{U}\|_X + \|p - P\|_M \leq K(h_1^{k_1} + h_2^{k_2+1} + h_2^{l_2+1}), \tag{3.3}$$

assuming $\mathbf{u}$ and p are smooth enough, where

$$\|\mathbf{v}\|_X^2 = \|\mathbf{v}_1\|_{H^1(\Omega_1)}^2 + \|\mathbf{v}_2\|_{L^2(\Omega_2)}^2 + \|\nabla \cdot \mathbf{v}_2\|_{L^2(\Omega_2)}^2, \quad \|w\|_M = \|w\|_{L^2(\Omega)}.$$

The results easily extend to the non-homogeneous case considered here.

Since $\mathbf{U} \cdot \mathbf{n}$ is used in the inflow boundary condition for the transport equation, it is important that it approximates $\mathbf{u} \cdot \mathbf{n}$ accurately on Γ_{in}. In particular, we assume that

$$\|(\mathbf{u} - \mathbf{U}) \cdot \mathbf{n}\|_{\Gamma_{in}} \leq K(h_1^{k_1+1} + h_2^{k_2+2}). \tag{3.4}$$

On $\Gamma_1 \cap \Gamma_{in}$ this is satisfied due to the approximation properties of $Q_{h,1}$. To satisfy (3.4) on $\Gamma_2 \cap \Gamma_{in}$ we need to postprocess $\mathbf{U}$ on each element $E \in \mathcal{T}_{h,2}$ such that $E \cap \Gamma_{in} \neq \emptyset$. To be precise let us denote the velocity mixed finite element space on E by $\mathbf{X}_{h,2}^{k_2}(E)$. Since $\mathbf{X}_{h,2}^{k_2}(E) \subset \mathbf{X}_{h,2}^{k_2+1}(E)$, we have that $\mathbf{U} \in \mathbf{X}_{h,2}^{k_2+1}(E)$. Let $\tilde{\mathbf{U}} \in \mathbf{X}_{h,2}^{k_2+1}(E)$ be such that $\tilde{\mathbf{U}}$ agrees with $\mathbf{U}$ at all finite element nodes that are not on Γ_{in} and $\tilde{\mathbf{U}} \cdot \mathbf{n}_2 = Q_{h,2}^{k_2+1} g_2$ on $\partial E \cap \Gamma_{in}$. Clearly the postprocessed velocity satisfies (3.4). Moreover, the normal velocity on all interior edges (faces) of E is preserved and the error bound (3.3) still holds. From a computational point of view, only the integrals on Γ_{in} in the transport scheme are affected by this postprocessing. To keep the notation simple, in the following $\mathbf{U}$ will denote the postprocessed velocity.

4 Formulation of the LDG method for transport

We rewrite the transport equation in a mixed form by introducing the diffusive flux

$$\mathbf{z} = -\mathbf{D}\nabla c. \tag{4.1}$$

The system (2.11)-(2.14) is equivalent to

$$\phi c_t + \nabla \cdot (c\mathbf{u} + \mathbf{z}) = \phi s, \tag{4.2}$$

$$(c\mathbf{u} + \mathbf{z}) \cdot \mathbf{n} = c_{in} \mathbf{u} \cdot \mathbf{n} \quad \text{on } \Gamma_{in}, \tag{4.3}$$

$$\mathbf{z} \cdot \mathbf{n} = 0 \quad \text{on } \Gamma_{out}. \tag{4.4}$$

Let $\mathcal{T}_h$ be a shape-regular finite element partition of Ω. We denote by h_E the diameter of an element E and set h to be the maximum element diameter. We assume that no element E overlaps with both Γ_{in} and Γ_{out} and that each element E has a Lipschitz boundary ∂E. The partition $\mathcal{T}_h$ may be different from $\mathcal{T}_{h,1}$ and $\mathcal{T}_{h,2}$. Let $W_E = H^1(E)$, $\mathbf{V}_E = (W_E)^d$, and let $\mathbf{n}_E$ be the outward unit normal on ∂E. We will need some notation for values of discontinuous functions on element edges (faces in 3D). Let

$$W = \left\{ w \in L^2(\Omega) : \text{on each } E \in \mathcal{T}_h,\ w \in W_E \right\},$$

$$\mathbf{V} = \{ \mathbf{v} \in (L^2(\Omega))^d : \text{on each } E \in \mathcal{T}_h,\ \mathbf{v} \in \mathbf{V}_E \}.$$

Let $w \in W$. For any $E \in \mathcal{T}_h$ and any $\mathbf{x} \in \partial E$ we define

$$w^-(\mathbf{x}) = \lim_{s \to 0^-} w(\mathbf{x} + s\,\mathbf{n}_E), \quad w^+(\mathbf{x}) = \lim_{s \to 0^+} w(\mathbf{x} + s\,\mathbf{n}_E), \tag{4.5}$$

$$\overline{w}(\mathbf{x}) = \frac{1}{2}\left(w^+(\mathbf{x}) + w^-(\mathbf{x})\right), \quad \text{and} \quad w^u(\mathbf{x}) = \begin{cases} w^-(\mathbf{x}) & \text{if } \mathbf{u}\cdot\mathbf{n}_E \geq 0 \\ w^+(\mathbf{x}) & \text{if } \mathbf{u}\cdot\mathbf{n}_E < 0 \end{cases}. \tag{4.6}$$

For a vector function $\mathbf{v} \in \mathbf{V}$, $\mathbf{v}^-$, $\mathbf{v}^+$, and $\overline{\mathbf{v}}$ are defined in a similar way.

Assuming that the solution to (4.2)–(4.4) is smooth enough, multiplying by appropriate test functions on every element E and integrating by parts, we obtain the following weak formulation. For every $E \in \mathcal{T}_h$, $c \in W_E$ and $\mathbf{z} \in \mathbf{V}_E$ satisfy

$$\left(\mathbf{D}^{-1}\mathbf{z}, \mathbf{v}\right)_E - (c, \nabla\cdot\mathbf{v})_E + \left\langle c, \mathbf{v}^-\cdot\mathbf{n}_E\right\rangle_{\partial E} = 0, \ \forall\, \mathbf{v} \in \mathbf{V}_E, \tag{4.7}$$

$$\begin{aligned}(\phi c_t, w)_E - (c\mathbf{u} + \mathbf{z}, \nabla w)_E + \left\langle (c\mathbf{u} + \mathbf{z})\cdot\mathbf{n}_E, w^-\right\rangle_{\partial E\setminus\Gamma} + \left\langle c\mathbf{u}\cdot\mathbf{n}_E, w^-\right\rangle_{\partial E\cap\Gamma_{out}} \\ = (\phi s, w)_E - \left\langle c_{in}\mathbf{u}\cdot\mathbf{n}_E, w^-\right\rangle_{\partial E\cap\Gamma_{in}}, \ \forall\, w \in W_E.\end{aligned} \tag{4.8}$$

Let $W_{h,E} \subset W_E$ denote the space of all polynomials on E of degree $\leq k_E$, $k_E \geq 1$, and let $\mathbf{V}_{h,E} = (W_{h,E})^d$. Let $k = \min_E k_E$. On each element E, $c(\cdot,t)$ and $\mathbf{z}(\cdot,t)$ are approximated by $C(\cdot,t) \in W_{h,E}$ and $\mathbf{Z}(\cdot,t) \in \mathbf{V}_{h,E}$ respectively. Let

$$W_h := \left\{w \in L^2(\Omega) : \text{on each } E \in \mathcal{T}_h,\ w \in W_{h,E}\right\},$$

$$\mathbf{V}_h := \{\mathbf{v} \in (L^2(\Omega))^d : \text{on each } E \in \mathcal{T}_h,\ \mathbf{v} \in \mathbf{V}_{h,E}\}.$$

Let $C^0 \in W_h$ be the L^2-projection of c^0:

$$\forall E \in \mathcal{T}_h, \quad \left(C^0 - c^0, w\right)_E \ = \ 0\ ,\ \forall\, w \in W_{h,E}. \tag{4.9}$$

The semi-discrete LDG method is defined as follows: for each $t \in [0,T]$ find $C(\cdot,t) \in W_h$ and $\mathbf{Z}(\cdot,t) \in \mathbf{V}_h$ such that on each $E \in \mathcal{T}_h$

$$\begin{aligned}\left(\mathbf{D}^{-1}\mathbf{Z}, \mathbf{v}\right)_E - (C, \nabla\cdot\mathbf{v})_E + \left\langle \overline{C}, \mathbf{v}^-\cdot\mathbf{n}_E\right\rangle_{\partial E\setminus\Gamma} \\ + \left\langle C^-, \mathbf{v}^-\cdot\mathbf{n}_E\right\rangle_{\partial E\cap\Gamma} = 0, \ \forall\, \mathbf{v} \in \mathbf{V}_{h,E},\ t \in [0,T),\end{aligned} \tag{4.10}$$

$$\begin{aligned}(\phi C_t, w)_E - (C\mathbf{U} + \mathbf{Z}, \nabla w)_E + \left\langle (C^u\mathbf{U} + \overline{\mathbf{Z}})\cdot\mathbf{n}_E, w^-\right\rangle_{\partial E\setminus\Gamma} \\ + \left\langle C^-\mathbf{U}\cdot\mathbf{n}_E, w^-\right\rangle_{\partial E\cap\Gamma_{out}} = (\phi s, w)_E \\ - \left\langle c_{in}\mathbf{U}\cdot\mathbf{n}_E, w^-\right\rangle_{\partial E\cap\Gamma_{in}}, \forall\, w \in W_{h,E},\ t \in (0,T),\end{aligned} \tag{4.11}$$

$$C(\cdot,0) = C^0. \tag{4.12}$$

In the above scheme we assume that high enough quadrature rules are used, so that the numerical integration error is dominated by the discretization error. Note that the computed velocity $\mathbf{U}$ is needed to evaluate element and edge integrals in (4.11). As a result $\mathbf{U}$ needs to be evaluated at any quadrature point in E or on ∂E. Since we allow for the flow and transport grids to differ and the velocity approximation could be discontinuous, $\mathbf{U}$ may not be well defined at a given quadrature point. This problem is handled by decomposing E

into sub-elements according to its intersection with the flow grid. More precisely, let $E_i^{X_h}$, $i = 1, \ldots, m_E$ be the elements of the flow grid that overlap with E. Then we have

$$\int_E \varphi \, d\mathbf{x} = \sum_{i=1}^{m_E} \int_{E \cap E_i^{X_h}} \varphi \, d\mathbf{x}, \qquad \int_{\partial E} \varphi \, d\sigma = \sum_{i=1}^{m_E} \int_{\partial E \cap E_i^{X_h}} \varphi \, d\sigma.$$

The computed velocity $\mathbf{U}$ is well defined on all sub-elements and sub-edges.

In this paper we restrict our attention to the semi-discrete formulation. Standard methods such as Euler or Runge-Kutta can be employed for the time discretization, see, e.g. [16].

5 Stability of the LDG scheme

The stability argument is based on the analysis in [13]. The main difference here is that we allow for velocity with non-zero divergence.

By adding equations (4.10) and (4.11), summing over all the elements and integrating over t, we obtain the equivalent formulation

$$\begin{gathered} B_{\mathbf{U}}(C, \mathbf{Z}; w, \mathbf{v}) = -\int_0^T \left\langle c_{in} \mathbf{U} \cdot \mathbf{n}, w^- \right\rangle_{\Gamma_{in}} dt + \int_0^T (\phi s, w) \, dt, \\ \forall \, (w, \mathbf{v}) \in \mathcal{C}^0(0, T; W_h \times \mathbf{V}_h), \end{gathered} \tag{5.1}$$

where

$$\begin{aligned} B_{\mathbf{U}}(C, \mathbf{Z}; w, \mathbf{v}) := \int_0^T \sum_E \big\{ & (\phi C_t, w)_E - (C\mathbf{U} + \mathbf{Z}, \nabla w)_E \\ & + \left\langle C^- \mathbf{U} \cdot \mathbf{n}_E, w^- \right\rangle_{\partial E \cap \Gamma_{out}} + \left\langle (C^u \mathbf{U} + \overline{\mathbf{Z}}) \cdot \mathbf{n}_E, w^- \right\rangle_{\partial E \setminus \Gamma} + \left(\mathbf{D}^{-1} \mathbf{Z}, \mathbf{v}\right)_E \\ & - (C, \nabla \cdot \mathbf{v})_E + \left\langle \overline{C}, \mathbf{v}^- \cdot \mathbf{n}_E \right\rangle_{\partial E \setminus \Gamma} + \left\langle C^-, \mathbf{v}^- \cdot \mathbf{n}_E \right\rangle_{\partial E \cap \Gamma} \big\} dt. \end{aligned} \tag{5.2}$$

Taking $w = C$ and $\mathbf{v} = \mathbf{Z}$, we have

$$B_{\mathbf{U}}(C, \mathbf{Z}; C, \mathbf{Z}) = \Theta_1 + \Theta_2 + \Theta_3, \tag{5.3}$$

where

$$\begin{aligned} \Theta_1 &= \int_0^T \sum_E \big\{ (\phi C_t, C)_E + (\mathbf{D}^{-1} \mathbf{Z}, \mathbf{Z})_E \big\} dt, \\ \Theta_2 &= \int_0^T \sum_E \big\{ -(C\mathbf{U}, \nabla C)_E + \langle C^u \mathbf{U} \cdot \mathbf{n}_E, C^- \rangle_{\partial E \setminus \Gamma} + \langle C^- \mathbf{U} \cdot \mathbf{n}_E, C^- \rangle_{\partial E \cap \Gamma_{out}} \big\} dt, \\ \Theta_3 &= \int_0^T \sum_E \big\{ -(\mathbf{Z}, \nabla C)_E + \langle \overline{\mathbf{Z}} \cdot \mathbf{n}_E, C^- \rangle_{\partial E \setminus \Gamma} - (C, \nabla \cdot \mathbf{Z})_E \\ &\qquad\qquad + \langle \overline{C}, \mathbf{Z}^- \cdot \mathbf{n}_E \rangle_{\partial E \setminus \Gamma} + \langle C^-, \mathbf{Z}^- \cdot \mathbf{n}_E \rangle_{\partial E \cap \Gamma} \big\} dt. \end{aligned} \tag{5.4}$$

Since

$$(\phi C_t, C)_E = \frac{1}{2}\frac{d}{dt}(\phi^{1/2}C, \phi^{1/2}C)_E$$

we can write

$$\Theta_1 = \frac{1}{2}\|\phi^{1/2}C(T)\|^2 - \frac{1}{2}\|\phi^{1/2}C(0)\|^2 + \int_0^T \|\mathbf{D}^{-1/2}\mathbf{Z}\|^2 dt. \tag{5.5}$$

We continue with the bound on Θ_2. Integration by parts gives

$$(C\mathbf{U}, \nabla C)_E = \frac{1}{2}\int_{\partial E}(C^-)^2\mathbf{U}\cdot\mathbf{n}_E\, d\sigma - \frac{1}{2}\int_E C^2\nabla\cdot\mathbf{U}\, d\mathbf{x}.$$

Then we have

$$\begin{aligned}
\Theta_2 = \int_0^T \sum_E \Big\{ & -\frac{1}{2}\langle C^-\mathbf{U}\cdot\mathbf{n}_E, C^-\rangle_{\partial E\setminus\Gamma} - \frac{1}{2}\langle C^-\mathbf{U}\cdot\mathbf{n}_E, C^-\rangle_{\partial E\cap\Gamma_{in}} \\
& + \frac{1}{2}\langle C^-\mathbf{U}\cdot\mathbf{n}_E, C^-\rangle_{\partial E\cap\Gamma_{out}} + \frac{1}{2}(C^2, \nabla\cdot\mathbf{U})_E + \langle C^u\mathbf{U}\cdot\mathbf{n}_E, C^-\rangle_{\partial E\setminus\Gamma}\Big\}\, dt \\
= \int_0^T \sum_E \Big\{ & \frac{1}{2}(C^2, \nabla\cdot\mathbf{U})_E + \frac{1}{2}\langle|\mathbf{U}\cdot\mathbf{n}_E|, (C^-)^2\rangle_{\partial E\cap\Gamma} \\
& + \langle(C^u - \frac{1}{2}C^-)\mathbf{U}\cdot\mathbf{n}_E, C^-\rangle_{\partial E\setminus\Gamma}\Big\}\, dt \\
= \int_0^T \Big\{ & \frac{1}{2}(C^2, \nabla\cdot\mathbf{U}) + \frac{1}{2}\langle|\mathbf{U}\cdot\mathbf{n}|, (C^-)^2\rangle_\Gamma \\
& + \sum_E \langle(C^u - \frac{1}{2}C^-)\mathbf{U}\cdot\mathbf{n}_E, C^-\rangle_{\partial E\setminus\Gamma}\Big\}\, dt.
\end{aligned} \tag{5.6}$$

It is convenient to express the sum over the elements in the last term in (5.6) as a sum over the interior element edges (faces) $\{e\}$. Let $e \in \partial E$ be an interior edge (face) of the element E. For $w \in W_h$ and $\mathbf{v} \in \mathbf{V}_h$ we set on e

$$[w] = (w^- - w^+)\mathbf{n}_E, \quad [\mathbf{v}] = (\mathbf{v}^- - \mathbf{v}^+)\cdot\mathbf{n}_E.$$

Note that these definitions do not depend on which element E is taken as a reference. Let us also fix arbitrarily a unit normal vector on e, denoted by $\mathbf{n}_e$.

Since

$$\frac{1}{2}[C^2] = \frac{1}{2}((C^-)^2 - (C^+)^2)\mathbf{n}_E = \frac{1}{2}(C^- + C^+)(C^- - C^+)\mathbf{n}_E = \overline{C}[C],$$

we can write

$$
\begin{aligned}
\sum_E \langle (C^u - \frac{1}{2}C^-)\mathbf{U}\cdot\mathbf{n}_E, C^-\rangle_{\partial E\setminus\Gamma} &= \sum_e \langle \mathbf{U}\cdot(C^u[C] - \frac{1}{2}[C^2]), 1\rangle_e \\
&= \sum_e \langle \mathbf{U}\cdot(C^u[C] - \overline{C}[C]), 1\rangle_e \\
&= \sum_e \langle \mathbf{U}\cdot[C](C^u - \overline{C}), 1\rangle_e \\
&= \frac{1}{2}\sum_e \langle |\mathbf{U}\cdot\mathbf{n}_e|, [C]\cdot[C]\rangle_e,
\end{aligned}
\tag{5.7}
$$

where we used in the last equality that on any $e \in \partial E$

$$
\begin{aligned}
\mathbf{U}\cdot[C](C^u - \overline{C}) &= \mathbf{U}\cdot\mathbf{n}_E(C^- - C^+)\left(\left\{\begin{array}{l} C^-, \mathbf{U}\cdot\mathbf{n}_E \geq 0 \\ C^+, \mathbf{U}\cdot\mathbf{n}_E < 0 \end{array}\right\} - \frac{C^- + C^+}{2}\right) \\
&= \mathbf{U}\cdot\mathbf{n}_E(C^- - C^+)\frac{(C^- - C^+)}{2}\mathrm{sign}(\mathbf{U}\cdot\mathbf{n}_E) = \frac{1}{2}|\mathbf{U}\cdot\mathbf{n}_e|[C]\cdot[C].
\end{aligned}
$$

Substituting (5.7) into (5.6) we obtain

$$
\Theta_2 = \frac{1}{2}\int_0^T \left\{(C^2, \nabla\cdot\mathbf{U}) + \langle |\mathbf{U}\cdot\mathbf{n}|, (C^-)^2\rangle_\Gamma + \sum_e \langle |\mathbf{U}\cdot\mathbf{n}_e|, [C]\cdot[C]\rangle_e\right\} dt. \tag{5.8}
$$

To estimate Θ_3 we use the Green's formula to obtain

$$
\begin{aligned}
\Theta_3 = \int_0^T \sum_E \Big\{ &-\langle \mathbf{Z}^-\cdot\mathbf{n}_E, C^-\rangle_{\partial E\setminus\Gamma} + \frac{1}{2}\left\langle (\mathbf{Z}^+ + \mathbf{Z}^-)\cdot\mathbf{n}_E, C^-\right\rangle_{\partial E\setminus\Gamma} \\
&+ \frac{1}{2}\left\langle C^+ + C^-, \mathbf{Z}^-\cdot\mathbf{n}_E\right\rangle_{\partial E\setminus\Gamma}\Big\}\, dt \\
= \int_0^T \sum_E &\left\{\frac{1}{2}\langle C^+, \mathbf{Z}^-\cdot\mathbf{n}_E\rangle_{\partial E\setminus\Gamma} + \frac{1}{2}\langle \mathbf{Z}^+\cdot\mathbf{n}_E, C^-\rangle_{\partial E\setminus\Gamma}\right\} dt \\
= 0,&
\end{aligned}
\tag{5.9}
$$

where the last equality follows from the fact that on each interior edge (face) the contributions from the two adjacent elements cancel, due to the opposite directions of the outward normal vectors.

A combination of (5.3), (5.5), (5.8), and (5.9) gives

$$
\begin{aligned}
B_{\mathbf{U}}(C, \mathbf{Z}; C, \mathbf{Z}) &= \frac{1}{2}\|\phi^{1/2}C(T)\|^2 - \frac{1}{2}\|\phi^{1/2}C(0)\|^2 + \int_0^T \|\mathbf{D}^{-1/2}\mathbf{Z}\|^2 dt \\
&+ \frac{1}{2}\int_0^T \left\{(C^2, \nabla\cdot\mathbf{U}) + \langle |\mathbf{U}\cdot\mathbf{n}|, (C^-)^2\rangle_\Gamma + \sum_e \langle |\mathbf{U}\cdot\mathbf{n}_e|, [C]\cdot[C]\rangle_e\right\} dt.
\end{aligned}
\tag{5.10}
$$

Combining (5.1) and (5.10), and using Young's inequality

$$ab \le \frac{\epsilon}{2}a^2 + \frac{1}{2\epsilon}b^2 \ \ , \ a, b \in \mathbb{R} \, , \epsilon > 0 \tag{5.11}$$

with $\epsilon = 1$, we obtain

$$\begin{aligned} &\frac{1}{2}\|\phi^{1/2}C(T)\|^2 + \int_0^T \|\mathbf{D}^{-1/2}\mathbf{Z}\|^2 dt \\ &\qquad \le \frac{1}{2}\|\phi^{1/2}C(0)\|^2 + \frac{1}{2}\int_0^T (C^2, (\nabla \cdot \mathbf{U})_-)\, dt \\ &\qquad\quad + \frac{1}{2}\int_0^T \langle |\mathbf{U}\cdot\mathbf{n}|, (c_{in})^2\rangle_{\Gamma_{in}}\, dt + \int_0^T \|\phi^{1/2}s\|\ \|\phi^{1/2}C\| dt, \end{aligned} \tag{5.12}$$

where

$$(\nabla \cdot \mathbf{U})_- := \begin{cases} 0, & \nabla\cdot\mathbf{U} \ge 0, \\ -\nabla\cdot\mathbf{U}, & \nabla\cdot\mathbf{U} < 0. \end{cases}$$

For the second term on the right in (5.12) we have

$$\frac{1}{2}\int_0^T (C^2, (\nabla \cdot \mathbf{U})_-)\, dt \le \frac{1}{2}\|\phi^{-1}(\nabla\cdot\mathbf{U})_-\|_{0,\infty}\int_0^T \|\phi^{1/2}C(t)\|^2\, dt,$$

and the use of Gronwall's inequality implies

$$\begin{aligned} &\|\phi^{1/2}C(T)\|^2 + 2\int_0^T \|\mathbf{D}^{-1/2}\mathbf{Z}\|^2 dt \\ &\le e^{LT}\left(\|\phi^{1/2}C(0)\|^2 + \int_0^T \langle |\mathbf{U}\cdot\mathbf{n}|, (c_{in})^2\rangle_{\Gamma_{in}}\, dt + 2\int_0^T \|\phi^{1/2}s\|\ \|\phi^{1/2}C\| dt\right), \end{aligned} \tag{5.13}$$

where

$$L := \|\phi^{-1}(\nabla\cdot\mathbf{U})_-\|_{0,\infty}. \tag{5.14}$$

Using (4.9),

$$\|\phi^{1/2}C(0)\| \le (\phi^*)^{1/2}\|c^0\|. \tag{5.15}$$

To complete the stability analysis we need the following result shown in [13].

Lemma 5.1 *Suppose that for all* $T > 0$

$$\chi^2(T) + R(T) \le A(T) + 2\int_0^T B(t)\chi(t)dt,$$

where R, A *and* B *are nonnegative functions. Then*

$$\sqrt{\chi^2 + R(T)} \le \sup_{0\le t\le T} A^{1/2}(t) + \int_0^T B(t)dt.$$

Let us define the norm $|||(C,\mathbf{Z})|||$ by

$$|||(C,\mathbf{Z})|||^2 := \|\phi^{1/2}C(T)\|^2 + 2\int_0^T \|\mathbf{D}^{-1/2}\mathbf{Z}\|^2 dt. \tag{5.16}$$

Then, using (5.13), (5.15), and Lemma 5.1, we obtain the following stability result.

Theorem 5.1 *The solution to the semi-discrete LDG method* (4.10)–(4.12) *satisfies*

$$|||(C,\mathbf{Z})||| \le e^{\frac{LT}{2}}\left(\phi^*\|c^0\|^2 + \int_0^T \langle|\mathbf{U}\cdot\mathbf{n}|,(c_{in})^2\rangle_{\Gamma_{in}}\,dt\right)^{1/2} + e^{LT}\int_0^T \|\phi^{1/2}s\|\,dt, \tag{5.17}$$

where L is defined in (5.14).

Remark 5.1 *The stability estimate above depends on $\|\nabla\cdot\mathbf{U}\|_{0,\infty}$ and $\|\mathbf{U}\cdot\mathbf{n}\|_{0,\infty,\Gamma_{in}}$. In Ω_1, L^∞ bounds on the computed Stokes velocity, see e.g. [22], can be used to control these terms by $\|\mathbf{u}\|_{1,\infty,\Omega_1}$. In Ω_2,* (3.2) *implies that $\nabla\cdot\mathbf{U}$ is the $L^2(\Omega_2)$ projection of $\nabla\cdot\mathbf{u}$ in $M_{h,2}$; therefore $\|\nabla\cdot\mathbf{U}\|_{0,\infty,\Omega_2} \le K\|\nabla\cdot\mathbf{u}\|_{0,\infty,\Omega_2}$. Similarly, since $\mathbf{U}\cdot\mathbf{n}_2 = Q_{h,2}\mathbf{u}\cdot\mathbf{n}_2$ on $\Gamma_2\cap\Gamma_{in}$, we have that $\|\mathbf{U}\cdot\mathbf{n}_2\|_{0,\infty,\Gamma_2\cap\Gamma_{in}} \le K\|\mathbf{u}\cdot\mathbf{n}_2\|_{0,\infty,\Gamma_2\cap\Gamma_{in}}$.*

6 Error analysis of the LDG scheme

Let $\Pi c \in W_h$, $\Pi\mathbf{z} \in \mathbf{V}_h$, and $\Pi\mathbf{u} \in \mathbf{V}_h$ denote the L^2-projections of c, $\mathbf{z}$, and $\mathbf{u}$, respectively:

$$\forall E \in \mathcal{T}_h, \quad (c - \Pi c, w)_E = 0\ ,\ \forall\, w \in W_{h,E}, \tag{6.1}$$
$$\forall E \in \mathcal{T}_h, \quad (\mathbf{z} - \Pi\mathbf{z}, \mathbf{v})_E = 0\ ,\ \forall\, \mathbf{v} \in \mathbf{V}_{h,E}, \tag{6.2}$$
$$\forall E \in \mathcal{T}_h, \quad (\mathbf{u} - \Pi\mathbf{u}, \mathbf{v})_E = 0\ ,\ \forall\, \mathbf{v} \in \mathbf{V}_{h,E}. \tag{6.3}$$

The L^2-projection has the approximation property [12]

$$\|q - \Pi q\|_{m,p,E} \le K h_E^{l-m}\|q\|_{l,p,E}, \quad 0 \le m \le l \le k_E + 1,\ 1 \le p \le \infty, \tag{6.4}$$

where q is either a scalar or a vector function. We will also make use of the trace inequality [3]

$$\forall\, e \in \partial E, \quad \|\chi\|_e \le\ K\left(h_E^{-1/2}\|\chi\|_E + h_E^{1/2}\,|\chi|_{1,E}\right) \qquad \forall\,\chi \in H^1(E). \tag{6.5}$$

Using (6.4) and (6.5),

$$\|q - \Pi q\|_e \le K h_E^{l-1/2}\|q\|_{l,E}, \quad 1 \le l \le k_E + 1. \tag{6.6}$$

For polynomial functions, (6.5) and the inverse inequality [12]

$$\|w\|_{1,E} \le K h_E^{-1}\|w\|_E. \tag{6.7}$$

imply

$$\|w\|_e \le K h_E^{-1/2} \|w\|_E. \tag{6.8}$$

Similarly to the discrete variational formulation (5.1), the weak solution of (4.7)–(4.8) satisfies

$$\begin{gathered} B_{\mathbf{u}}(c,\mathbf{z};w,\mathbf{v}) = -\int_0^T \left\langle c_{in}\mathbf{u}\cdot\mathbf{n}, w^-\right\rangle_{\Gamma_{in}} dt + \int_0^T (\phi s, w)\,dt, \\ \forall\,(w,\mathbf{v}) \in \mathcal{C}^0(0,T;W\times\mathbf{V}). \end{gathered} \tag{6.9}$$

Subtracting (5.1) from (6.9) gives

$$B_{\mathbf{u}}(c,\mathbf{z};w,\mathbf{v}) - B_{\mathbf{U}}(C,\mathbf{Z};w,\mathbf{v}) = -\int_0^T \left\langle c_{in}(\mathbf{u}-\mathbf{U})\cdot\mathbf{n}, w^-\right\rangle_{\Gamma_{in}} dt. \tag{6.10}$$

Let $\psi_c = C - \Pi c$, $\psi_{\mathbf{z}} = \mathbf{Z} - \Pi\mathbf{z}$, $\theta_c = c - \Pi c$, and $\theta_{\mathbf{z}} = \mathbf{z} - \Pi\mathbf{z}$. Setting $(w,\mathbf{v}) = (\psi_c, \psi_{\mathbf{z}})$ in (6.10), the expression on the left becomes

$$B_{\mathbf{u}}(\theta_c,\theta_{\mathbf{z}};\psi_c,\psi_{\mathbf{z}}) + B_{\mathbf{u}}(\Pi c,\Pi z;\psi_c,\psi_{\mathbf{z}}) - B_{\mathbf{U}}(\psi_c,\psi_{\mathbf{z}};\psi_c,\psi_{\mathbf{z}}) - B_{\mathbf{U}}(\Pi c,\Pi\mathbf{z};\psi_c,\psi_{\mathbf{z}}),$$

hence (6.10) can be written as

$$\begin{aligned} B_{\mathbf{U}}(\psi_c,\psi_{\mathbf{z}};\psi_c,\psi_{\mathbf{z}}) &= B_{\mathbf{u}}(\theta_c,\theta_{\mathbf{z}};\psi_c,\psi_{\mathbf{z}}) + B_{\mathbf{u}}(\Pi c,\Pi\mathbf{z};\psi_c,\psi_{\mathbf{z}}) \\ &\quad - B_{\mathbf{U}}(\Pi c,\Pi\mathbf{z};\psi_c,\psi_{\mathbf{z}}) + \int_0^T \left\langle c_{in}(\mathbf{u}-\mathbf{U})\cdot\mathbf{n}, \psi_c^-\right\rangle_{\Gamma_{in}} dt. \end{aligned} \tag{6.11}$$

For the error due to the velocity approximation we have

$$\begin{aligned} &B_{\mathbf{u}}(\Pi c,\Pi\mathbf{z};\psi_c,\psi_{\mathbf{z}}) - B_{\mathbf{U}}(\Pi c,\Pi\mathbf{z};\psi_c,\psi_{\mathbf{z}}) \\ &\quad= \int_0^T \sum_E \{-(\Pi c(\mathbf{u}-\mathbf{U}), \nabla\psi_c)_E + \langle(\Pi c)^u\,(\mathbf{u}-\mathbf{U})\cdot\mathbf{n}_E, \psi_c^-\rangle_{\partial E\setminus\Gamma} \\ &\qquad\quad + \langle(\Pi c)^-(\mathbf{u}-\mathbf{U})\cdot\mathbf{n}_E, \psi_c^-\rangle_{\partial E\cap\Gamma_{out}}\}\,dt \\ &\quad= \int_0^T \sum_E \{(\nabla\cdot(\Pi c(\mathbf{u}-\mathbf{U})), \psi_c)_E + \langle((\Pi c)^u - (\Pi c)^-)(\mathbf{u}-\mathbf{U})\cdot\mathbf{n}_E, \psi_c^-\rangle_{\partial E\setminus\Gamma} \\ &\qquad\quad - \langle(\Pi c)^-(\mathbf{u}-\mathbf{U})\cdot\mathbf{n}_E, \psi_c^-\rangle_{\partial E\cap\Gamma_{in}}\}\,dt. \end{aligned} \tag{6.12}$$

Substituting (6.12) into (6.11) and using the definition (5.2) for $B_{\mathbf{u}}(\theta_c,\theta_{\mathbf{z}};\psi_c,\psi_{\mathbf{z}})$, we obtain

$$
\begin{aligned}
B_{\mathbf{U}}(\psi_c, \psi_{\mathbf{z}}; \psi_c, \psi_{\mathbf{z}}) = \int_0^T \sum_E \{ & (\phi(\theta_c)_t, \psi_c)_E - (\theta_c \mathbf{u}, \nabla \psi_c)_E - (\theta_{\mathbf{z}}, \nabla \psi_c)_E \\
& + \langle \theta_c^u \mathbf{u} \cdot \mathbf{n}_E, \psi_c^- \rangle_{\partial E \backslash \Gamma} + \langle \overline{\theta_{\mathbf{z}}} \cdot \mathbf{n}_E, \psi_c^- \rangle_{\partial E \backslash \Gamma} + \langle \theta_c^- \mathbf{u} \cdot \mathbf{n}_E, \psi_c^- \rangle_{\partial E \cap \Gamma_{out}} \\
& + (\mathbf{D}^{-1} \theta_{\mathbf{z}}, \psi_{\mathbf{z}})_E - (\theta_c, \nabla \cdot \psi_{\mathbf{z}})_E + \langle \overline{\theta_c}, \psi_{\mathbf{z}}^- \cdot \mathbf{n}_E \rangle_{\partial E \backslash \Gamma} + \langle \theta_c^-, \psi_{\mathbf{z}}^- \cdot \mathbf{n}_E \rangle_{\partial E \cap \Gamma} \\
& + (\nabla \cdot (\Pi c(\mathbf{u} - \mathbf{U})), \psi_c)_E + \langle ((\Pi c)^u - (\Pi c)^-)(\mathbf{u} - \mathbf{U}) \cdot \mathbf{n}_E, \psi_c^- \rangle_{\partial E \backslash \Gamma} \\
& + \langle (c_{in} - (\Pi c)^-)(\mathbf{u} - \mathbf{U}) \cdot \mathbf{n}_E, \psi_c^- \rangle_{\partial E \cap \Gamma_{in}} \} \, dt.
\end{aligned} \tag{6.13}
$$

We now rewrite the summation over the elements in (6.13) in terms of a summation over the interior edges (faces) where it is relevant:

$$
\begin{aligned}
B_{\mathbf{U}}(\psi_c, \psi_{\mathbf{z}}; \psi_c, \psi_{\mathbf{z}}) = \int_0^T \sum_E \{ & (\phi(\theta_c)_t, \psi_c)_E - (\theta_c \mathbf{u}, \nabla \psi_c)_E - (\theta_{\mathbf{z}}, \nabla \psi_c)_E \\
& + (\mathbf{D}^{-1} \theta_{\mathbf{z}}, \psi_{\mathbf{z}})_E - (\theta_c, \nabla \cdot \psi_{\mathbf{z}})_E + (\nabla \cdot (\Pi c(\mathbf{u} - \mathbf{U})), \psi_c)_E \\
& + \langle ((\Pi c)^u - (\Pi c)^-)(\mathbf{u} - \mathbf{U}) \cdot \mathbf{n}_E, \psi_c^- \rangle_{\partial E \backslash \Gamma} \} dt \\
& + \int_0^T \sum_e \{ \langle \theta_c^u \mathbf{u}, [\psi_c] \rangle_e + \langle \overline{\theta_{\mathbf{z}}}, [\psi_c] \rangle_e + \langle \overline{\theta_c}, [\psi_{\mathbf{z}}] \rangle_e \} \, dt \\
& + \int_0^T \{ \langle \theta_c^- \mathbf{u} \cdot \mathbf{n}, \psi_c^- \rangle_{\Gamma_{out}} + \langle \theta_c^-, \psi_{\mathbf{z}}^- \cdot \mathbf{n} \rangle_{\Gamma} \\
& + \langle (c_{in} - (\Pi c)^-)(\mathbf{u} - \mathbf{U}) \cdot \mathbf{n}, \psi_c^- \rangle_{\Gamma_{in}} \} \, dt \equiv T_1 + T_2 + ... + T_{13}.
\end{aligned} \tag{6.14}
$$

Using (5.10) and (4.9), (6.14) implies

$$
\frac{1}{2} \| \phi^{1/2} \psi_c(T) \|^2 + \int_0^T \| \mathbf{D}^{-1/2} \psi_{\mathbf{z}} \|^2 dt \le \frac{1}{2} \int_0^T (\psi_c^2, (\nabla \cdot \mathbf{U})_-) \, dt + T_1 + T_2 + ... + T_{13}. \tag{6.15}
$$

For the first term on the right above we have

$$
\frac{1}{2} \int_0^T (\psi_c^2, (\nabla \cdot \mathbf{U})_-) \, dt \le \frac{1}{2} \| \phi^{-1} (\nabla \cdot \mathbf{U})_- \|_{0,\infty} \int_0^T \| \phi^{1/2} \psi_c(t) \|^2 \, dt. \tag{6.16}
$$

We continue with bounds on the other terms on the right in (6.15).

From the definition of the L^2-projections (6.1) and (6.2) it follows that

$$
T_3 = T_5 = 0. \tag{6.17}
$$

Applying the Cauchy-Schwarz inequality, we obtain for T_1

$$
T_1 = \int_0^T (\phi^{1/2} (\theta_c)_t, \phi^{1/2} \psi_c) \, dt \le (\phi^*)^{1/2} \int_0^T \| (\theta_c)_t \| \, \| \phi^{1/2} \psi_c \| \, dt. \tag{6.18}
$$

For the bound of T_2 we will use the L^2-projection of $\mathbf{u}$ onto the space of piecewise constant vectors $\Pi_0\mathbf{u}$ satisfying

$$\forall E \in \mathcal{T}_h, \quad (\mathbf{u} - \Pi_0\mathbf{u}, 1)_E = 0, \quad \|\mathbf{u} - \Pi_0\mathbf{u}\|_{0,p,E} \le K h_E \|\mathbf{u}\|_{1,p,E}, \ 1 \le p \le \infty.$$

Using (6.1) we have

$$\begin{aligned} T_2 &= -\int_0^T \sum_E (\theta_c\mathbf{u}, \nabla\psi_c)_E \, dt = \int_0^T \sum_E (\theta_c(\Pi_0\mathbf{u} - \mathbf{u}), \nabla\psi_c)_E \, dt \\ &\le K\|\mathbf{u}\|_{1,\infty} \int_0^T \sum_E h_E \|\theta_c\|_E \|\nabla\psi_c\|_E \, dt \le K\|\mathbf{u}\|_{1,\infty} \int_0^T \sum_E \|\theta_c\|_E \|\psi_c\|_E \, dt \\ &\le K\|\mathbf{u}\|_{1,\infty} \phi_*^{-1/2} \int_0^T \|\theta_c\| \|\phi^{1/2}\psi_c\| \, dt, \end{aligned} \tag{6.19}$$

where we used (6.7) for the second inequality. Handling T_4 is straightforward, using (5.11) with $\epsilon = 1/2$:

$$T_4 = \int_0^T \sum_E (\mathbf{D}^{-1}\theta_{\mathbf{z}}, \psi_{\mathbf{z}})_E \, dt \le \int_0^T \|\mathbf{D}^{-1/2}\theta_{\mathbf{z}}\|^2 dt + \frac{1}{4}\int_0^T \|\mathbf{D}^{-1/2}\psi_{\mathbf{z}}\|^2 dt. \tag{6.20}$$

Using (6.4), we have for T_6:

$$\begin{aligned} T_6 &= \int_0^T \sum_E (\nabla \cdot (\Pi c(\mathbf{u} - \mathbf{U})), \psi_c)_E \, dt \\ &= \int_0^T \sum_E \{(\nabla \Pi c \cdot (\mathbf{u} - \mathbf{U}), \psi_c)_E + (\Pi c \nabla \cdot (\mathbf{u} - \mathbf{U}), \psi_c)_E\} \, dt \\ &\le \ \phi_*^{-1/2} \int_0^T \sum_E (\|\nabla\Pi c\|_{0,\infty,E} \|\mathbf{u} - \mathbf{U}\|_E + \|\Pi c\|_{0,\infty,E} \|\nabla \cdot (\mathbf{u} - \mathbf{U})\|_E) \|\phi^{1/2}\psi_c\|_E \, dt \\ &\le K\phi_*^{-1/2} \int_0^T \|c\|_{1,\infty} \|\mathbf{u} - \mathbf{U}\|_X \|\phi^{1/2}\psi_c\| \, dt. \end{aligned} \tag{6.21}$$

For T_7 we have

$$\begin{aligned} T_7 &= \int_0^T \sum_E \langle ((\Pi c)^u - (\Pi c)^-)(\mathbf{u} - \mathbf{U}) \cdot \mathbf{n}_E, \psi_c^- \rangle_{\partial E \setminus \Gamma} \, dt \\ &\le \int_0^T \sum_E \|(\Pi c)^u - (\Pi c)^-\|_{0,\infty,\partial E\setminus\Gamma} \|(\mathbf{u} - \mathbf{U}) \cdot \mathbf{n}_E\|_{\partial E\setminus\Gamma} \|\psi_c^-\|_{\partial E\setminus\Gamma} \, dt. \end{aligned} \tag{6.22}$$

Note that

$$\|(\Pi c)^u - (\Pi c)^-\|_{0,\infty,\partial E} \le \|(\Pi c)^u - c\|_{0,\infty,\partial E} + \|c - (\Pi c)^-\|_{0,\infty,\partial E} \le \|c - \Pi c\|_{0,\infty,\delta(E)},$$

where $\delta(E)$ is the union of all elements that share an edge (face) with E. For the second term on the right in (6.22) we have

$$\begin{aligned}
\|(\mathbf{u}-\mathbf{U})\cdot\mathbf{n}_e\|_e &\le \|(\mathbf{u}-\Pi\mathbf{u})\cdot\mathbf{n}_e\|_e + \|(\Pi\mathbf{u}-\mathbf{U})\cdot\mathbf{n}_e\|_e \\
&\le K(\|(\mathbf{u}-\Pi\mathbf{u})\cdot\mathbf{n}_e\|_e + h_E^{-1/2}\|\Pi\mathbf{u}-\mathbf{U}\|_E) \\
&\le K(\|(\mathbf{u}-\Pi\mathbf{u})\cdot\mathbf{n}_e\|_e + h_E^{-1/2}\|\mathbf{u}-\Pi\mathbf{u}\|_E + h_E^{-1/2}\|\mathbf{u}-\mathbf{U}\|_E),
\end{aligned}$$

where second inequality follows from an application of (6.8). Therefore for T_7 we obtain, using (6.8) again,

$$\begin{aligned}
T_7 \le K\int_0^T \|\theta_c\|_{0,\infty}\sum_E(&\|(\mathbf{u}-\Pi\mathbf{u})\cdot\mathbf{n}_E\|_{\partial E\setminus\Gamma} + h_E^{-1/2}\|\mathbf{u}-\Pi\mathbf{u}\|_E \\
&+ h_E^{-1/2}\|\mathbf{u}-\mathbf{U}\|_E)h_E^{-1/2}\|\psi_c\|_E \\
\le K\phi_*^{-1/2}\int_0^T &\|c\|_{1,\infty}(h^{1/2}\|(\mathbf{u}-\Pi\mathbf{u})\cdot\mathbf{n}\|_{\mathcal{E}_h} + \|\mathbf{u}-\Pi\mathbf{u}\| + \|\mathbf{u}-\mathbf{U}\|)\|\phi^{1/2}\psi_c\|,
\end{aligned} \tag{6.23}$$

where $\|w\|_{\mathcal{E}_h} = (\sum_e \|w\|_e^2)^{1/2}$. Similarly, for T_8 we have

$$\langle\theta_c^u\mathbf{u},[\psi_c]\rangle_e \le K\phi_*^{-1/2}\|\mathbf{u}\cdot\mathbf{n}_e\|_{0,\infty,e}\|\theta_c^u\|_e h_E^{-1/2}\|\phi^{1/2}\psi_c\|_E,$$

therefore

$$T_8 \le K\|\mathbf{u}\|_{0,\infty}\phi_*^{-1/2}\int_0^T h^{-1/2}\|\theta_c^u\|_{\mathcal{E}_h}\|\phi^{1/2}\psi_c\|. \tag{6.24}$$

Similarly,

$$T_9 \le K\phi_*^{-1/2}\int_0^T h^{-1/2}\|\overline{\theta_{\mathbf{z}}}\cdot\mathbf{n}\|_{\mathcal{E}_h}\|\phi^{1/2}\psi_c\|, \tag{6.25}$$

and

$$\begin{aligned}
T_{10} &= \int_0^T \sum_e \langle\overline{\theta_c},[\psi_{\mathbf{z}}]\rangle_e\, dt \\
&\le K(D^*)^{1/2}\int_0^T h^{-1/2}\|\overline{\theta_c}\|_{\mathcal{E}_h}\|\mathbf{D}^{-1/2}\psi_{\mathbf{z}}\|\, dt \\
&\le K^2D^*\int_0^T h^{-1}\|\overline{\theta_c}\|_{\mathcal{E}_h}^2\, dt + \frac{1}{4}\int_0^T \|\mathbf{D}^{-1/2}\psi_{\mathbf{z}}\|^2\, dt,
\end{aligned} \tag{6.26}$$

using (5.11) with $\epsilon = 1/2$ for the last inequality. In a similar way we obtain

$$T_{11} \le K\|\mathbf{u}\|_{0,\infty}\phi_*^{-1/2}\int_0^T h^{-1/2}\|\theta_c^-\|_{\Gamma_{out}}\|\phi^{1/2}\psi_c\|\, dt, \tag{6.27}$$

$$T_{12} \le KD^* \int_0^T h^{-1} \|\theta_c^-\|_\Gamma^2 \, dt + \frac{1}{4} \int_0^T \|\mathbf{D}^{-1/2} \psi_{\mathbf{z}}\|^2 \, dt, \tag{6.28}$$

and

$$T_{13} \le K\phi_*^{-1/2} \int_0^T (\|c_{in}\|_{0,\infty,\Gamma_{in}} + \|c\|_{0,\infty,\Gamma_{in}}) h^{-1/2} \|(\mathbf{u} - \mathbf{U}) \cdot \mathbf{n}\|_{\Gamma_{in}} \|\phi^{1/2} \psi_c\| \, dt. \tag{6.29}$$

A combination of (6.15)–(6.29), the use of Gronwall's inequality for the term in (6.16), and an application of Lemma 5.1 imply

$$\begin{aligned} |||(\psi_c, \psi_{\mathbf{z}})||| \le K \int_0^T \big(& \|\mathbf{D}^{-1/2} \theta_{\mathbf{z}}\| + h^{-1/2} \|\overline{\theta_c}\|_{\mathcal{E}_h} + h^{-1/2} \|\theta_c^-\|_\Gamma \\ & + \|(\theta_c)_t\| + \|\theta_c\| + \|\mathbf{u} - \mathbf{U}\|_X + h^{1/2} \|(\mathbf{u} - \Pi\mathbf{u}) \cdot \mathbf{n}\|_{\mathcal{E}_h} \\ & + \|\mathbf{u} - \Pi\mathbf{u}\| + \|\mathbf{u} - \mathbf{U}\| + h^{-1/2} \|\theta_c^u\|_{\mathcal{E}_h} + h^{-1/2} \|\overline{\theta_{\mathbf{z}}} \cdot \mathbf{n}\|_{\mathcal{E}_h} \\ & + h^{-1/2} \|\theta_c^-\|_{\Gamma_{out}} + h^{-1/2} \|(\mathbf{u} - \mathbf{U}) \cdot \mathbf{n}\|_{\Gamma_{in}} \big) \, dt, \end{aligned} \tag{6.30}$$

where $K = K(e^{LT})$. The above bound, combined with the velocity error bounds (3.3) and (3.4) and the approximation properties (6.4) and (6.6), implies the following convergence result.

Theorem 6.1 *If the solution to the coupled system* (2.1)–(2.14) *is smooth enough, then the solution to the semi-discrete transport LDG method* (4.10)–(4.12) *satisfies*

$$|||(c - C, \mathbf{z} - \mathbf{Z})||| \le K(h^k + h_1^{k_1} + h_2^{k_2+1} + h_2^{l_2+1}). \tag{6.31}$$

7 Numerical results

In this section we present results from several computational experiments. The first three confirm the theoretical convergence rates for problems with given analytical solutions, while the last two illustrate the behavior of the method for realistic problems of coupled surface-subsurface flows with contaminant transport. In all tests the computational domain is taken to be $\Omega = \Omega_1 \cup \Omega_2$, where $\Omega_1 = [0,1] \times [\frac{1}{2}, 1]$ and $\Omega_2 = [0,1] \times [0, \frac{1}{2}]$. For simplicity we have used

$$\mathbf{T}(\mathbf{u}_1, p_1) = -p_1 \mathbf{I} + \mu \nabla \mathbf{u}_1$$

in the Stokes equation in Ω_1. The flow equations are solved via domain decomposition using the Taylor-Hood triangular finite elements in Ω_1 and the lowest order Raviart Thomas rectangular finite elements in Ω_2. In the LDG discretization of the transport equation we chose $W_{h,E}$ to be the space of bilinear functions on E. With these choices,

$$k_1 = 2, \quad k_2 = l_2 = 0, \quad \text{and} \quad k = 1.$$

The grid for the Stokes discretization in Ω_1 is obtained by first partitioning the domain into rectangles and then dividing each rectangle along its diagonal into two triangles. The flow grids in Ω_1 and Ω_2 match on the interface. The LDG transport grid on Ω is the rectangular grid used for the flow discretization (on Ω_1 this is the grid before subdividing into triangles).

The computed Stokes-Darcy velocity $\mathbf{U}$ is used in the transport scheme by first projecting it onto the space of piecewise bilinear functions on the transport grid. In the Stokes region the computed Taylor-Hood velocity vector is quadratic on each triangle and it is simply evaluated at the vertices of each rectangle. In the Darcy region the velocity vector at each vertex is recovered by combining the Raviart-Thomas normal velocities on the two edges forming the vertex.

7.1 Convergence tests

In the three convergence tests we use a second order Runge-Kutta method to discretize the transport equation in time. The final time is $T = 2$ and the time step is $\Delta t = 10^{-3}$, all numbers being dimensionless. The time step is chosen small enough so that the time discretization error is smaller than the spatial discretization error even for the finest grids used. In the convergence tests with nonzero diffusion we take $\mathbf{D} = 10^{-3}\,\mathbf{I}$, where $\mathbf{I}$ is the identity matrix. To handle the purely hyperbolic case $\mathbf{D} = 0$, we introduce an auxiliary variable $\tilde{\mathbf{z}} = -\nabla c$ and set $\mathbf{z} = \mathbf{D}\tilde{\mathbf{z}}$, following an approach from [2] for mixed finite element methods for elliptic problems. The LDG analysis for this formulation has been carried out in [13]. In all convergence tests we take $\phi = 1$.

The true solution of the transport equation for all three tests is

$$c(x, y, t) = t(\cos(\pi x) + \cos(\pi y))/\pi.$$

It is chosen to satisfy the outflow boundary condition (2.14) on $\partial\Omega$. The source function s is obtained by plugging into (2.11) the true solution functions for the concentration and the velocity specified below. The sign of the normal component of the true velocity determines whether the inflow or the outflow boundary condition is used for the transport equation. The initial condition function c^0 and the inflow condition function c_{in} are obtained by evaluating the true concentration at $t = 0$ and $\mathbf{x} \in \Gamma_{in}$, respectively.

In Test 1 the velocity field is chosen to be smooth across the interface:

$$\begin{aligned}
\mathbf{u}_1 = \mathbf{u}_2 &= \begin{bmatrix} sin(\frac{x}{G} + \omega)e^{y/G} \\ -cos(\frac{x}{G} + \omega)e^{y/G} \end{bmatrix}, \\
p_1 &= (\frac{G}{K} - \frac{\mu}{G})cos(\frac{x}{G} + \omega)e^{1/(2G)} + y - 0.5, \\
p_2 &= \frac{G}{K}cos(\frac{x}{G} + \omega)e^{y/G},
\end{aligned}$$

where

$$\mu = 0.1,\ K = 1,\ \alpha = 0.5,\ G = \frac{\sqrt{\mu K}}{\alpha},\ \text{and}\ \omega = 1.05.$$

The velocity $\mathbf{u}_1$ in the Stokes region is divergence free. The right hand sides $\mathbf{f}_1$ and $\mathbf{f}_2$ for the Stokes-Darcy flow system are obtained by plugging the above functions into (2.1) and (2.4), respectively. For the Stokes region, the velocity $\mathbf{u}_1$ is specified on the left and top boundaries, and the normal and tangential stresses $\mathbf{n}_1 \cdot \mathbf{T} \cdot \mathbf{n}_1$ and $\mathbf{n}_1 \cdot \mathbf{T} \cdot \boldsymbol{\tau}_1$ are specified on the right boundary. In the Darcy region, the normal velocity $\mathbf{u}_2 \cdot \mathbf{n}_2$ is specified on the left boundary and the pressure is specified on the bottom and right boundaries.

In Test 2 the velocity field is continuous, but not smooth, across the interface between the two subdomains:

$$
\begin{aligned}
\mathbf{u}_1 &= \begin{bmatrix} (2-x)(1.5-y)(y-\xi) \\ -\frac{y^3}{3} + \frac{y^2}{2}(\xi+1.5) - 1.5\xi y - 0.5 \end{bmatrix}, \\
\mathbf{u}_2 &= \begin{bmatrix} (2-x)(0.5-\xi) \\ \chi(y+0.5) \end{bmatrix}, \\
p_1 &= \frac{1}{K}(\frac{x^2}{2} - 2x)(0.5-\xi) - \frac{11\chi}{8K} + \mu(0.5-\xi) + y - 0.5, \\
p_2 &= \frac{1}{K}(\frac{x^2}{2} - 2x)(0.5-\xi) + \frac{\chi}{K}(-\frac{y^2+y}{2} - 1),
\end{aligned}
$$

where

$$
\xi = \frac{1-G}{2(1+G)}, \; \chi = \frac{-30\xi - 17}{48}, \; \beta = -0.3,
$$

and μ, K, α, and G are defined as in Test 1.

In Test 3 the normal velocity is continuous, but the tangential velocity is discontinuous across the interface:

$$
\begin{aligned}
\mathbf{u}_1 &= \begin{bmatrix} (2-x)(1.5-y)(y-\xi) \\ -\frac{y^3}{3} + \frac{y^2}{2}(\xi+1.5) - 1.5\xi y - 0.5 + \sin(\omega x) \end{bmatrix}, \\
\mathbf{u}_2 &= \begin{bmatrix} \omega\cos(\omega x) y \\ \chi(y+0.5) + \sin(\omega x) \end{bmatrix}, \\
p_1 &= -\frac{\sin(\omega x) + \chi}{2K} + \mu(0.5-\xi) + \cos(\pi y), \\
p_2 &= -\frac{\chi}{K}\frac{(y+0.5)^2}{2} - \frac{\sin(\omega x) y}{K},
\end{aligned}
$$

where $\omega = 6$ and the other parameters are defined as in Test 2.

In all three tests, the solutions are designed to satisfy the interface conditions (2.8)–(2.10).

The computed velocity field in Test 3 is shown in Figure 1. Note that the flow domain decomposition scheme correctly imposes continuity of the normal velocity, but allows for discontinuous tangential velocity across the interface.

The convergence rates for the transport equation are studied by solving the coupled flow-transport system on several levels of grid refinement. We test convergence with and

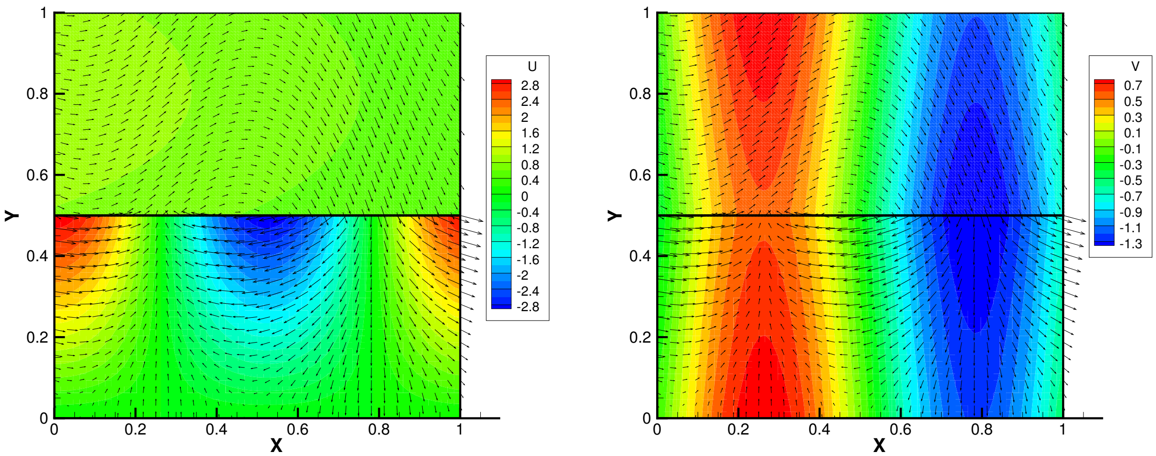

Figure 1: Computed velocity field in Test 3: discontinuous tangential velocity. Left: horizontal velocity; right: vertical velocity.

	$\mathbf{D} = 10^{-3}\,\mathbf{I}$				$\mathbf{D} = 0$	
mesh	$\lVert c - C \rVert_{L^\infty(L^2)}$	*rate*	$\lVert \mathbf{z} - \mathbf{Z} \rVert_{L^2(L^2)}$	*rate*	$\lVert c - C \rVert_{L^\infty(L^2)}$	*rate*
4x4	5.50e-02		5.31e-04		5.54e-02	
8x8	1.44e-02	1.93	2.39e-04	1.15	1.46e-02	1.93
16x16	3.75e-03	1.95	1.09e-04	1.13	3.81e-03	1.93
32x32	9.84e-04	1.93	5.09e-05	1.10	1.01e-03	1.92
64x64	2.60e-04	1.92	2.43e-05	1.07	2.71e-04	1.90

Table 1: Computed numerical errors and convergence rates for Test 1: smooth velocity.

without diffusion. The numerical errors and convergence rates for the three tests are reported in Tables 1,2, and 3. In all three cases we observe experimental convergence of order $O(h^2)$ for the concentration error in $L^\infty(0,T;L^2(\Omega))$ and approaching $O(h)$ for the diffusive flux error in $L^2(0,T;L^2(\Omega))$. Our theoretical results predict $O(h)$ for both variables. Similar second order convergence for the concentration has been observed numerically in the literature for the stand-alone transport equation, see e.g. [1]. Higher order convergence $O(h^{k+1})$ for the $L^2(0,T;L^2(\Omega))$ error of the concentration has been obtained theoretically by adding penalty terms [19, 9]. In our case there are additional terms contributing to the transport numerical error that are coming from the discretization error in the Stokes-Darcy velocity. For our particular choice of flow discretization these terms are $O(h^2)$ from Stokes and $O(h)$ from Darcy. The observed second order convergence of the concentration may be due to the superconvergence of the Raviart-Thomas velocity at the edge midpoints, which are used to obtain the bilinear velocity for the transport scheme. Further theoretical investigation of this phenomenon will be a topic of future work.

	$\mathbf{D} = 10^{-3}\,\mathbf{I}$				$\mathbf{D} = 0$	
$mesh$	$\|c - C\|_{L^\infty(L^2)}$	$rate$	$\|\mathbf{z} - \mathbf{Z}\|_{L^2(L^2)}$	$rate$	$\|c - C\|_{L^\infty(L^2)}$	$rate$
4x4	5.57e-02		4.33e-04		5.63e-02	
8x8	1.39e-02	2.00	2.01e-04	1.10	1.41e-02	2.00
16x16	3.48e-03	2.00	9.62e-05	1.07	3.51e-03	2.00
32x32	8.69e-04	2.00	4.70e-05	1.03	8.77e-04	2.00
64x64	2.17e-04	2.00	2.33e-05	1.01	2.19e-04	2.00

Table 2: Computed numerical errors and convergence rates for Test 2: continuous velocity.

	$\mathbf{D} = 10^{-3}\,\mathbf{I}$				$\mathbf{D} = 0$	
$mesh$	$\|c - C\|_{L^\infty(L^2)}$	$rate$	$\|\mathbf{z} - \mathbf{Z}\|_{L^2(L^2)}$	$rate$	$\|c - C\|_{L^\infty(L^2)}$	$rate$
4x4	1.99e+00		8.95e-03		2.07e+00	
8x8	3.27e-01	2.60	2.71e-03	1.72	3.39e-01	2.61
16x16	8.48e-02	1.95	1.20e-03	1.18	9.04e-02	1.91
32x32	2.23e-02	1.93	5.33e-04	1.17	2.59e-02	1.80
64x64	5.60e-03	2.00	1.77e-04	1.59	7.76e-03	1.74

Table 3: Computed numerical errors and convergence rates for Test 3: discontinuous tangential velocity.

7.2 Contaminant transport examples

We present two simulations of coupled surface-subsurface flow and contaminant transport. The Stokes region Ω_1 represents a lake or a river, which interacts with an aquifer occupying the Darcy region Ω_2. The porous medium is heterogeneous with permeability varying approximately two orders of magnitude, see Figure 2.

In both examples we use the following flow boundary conditions. In the Stokes region we set parabolic inflow on the left boundary, no normal flow and zero tangential stress on the top boundary, and zero normal and tangential stress on the right (outflow) boundary. In

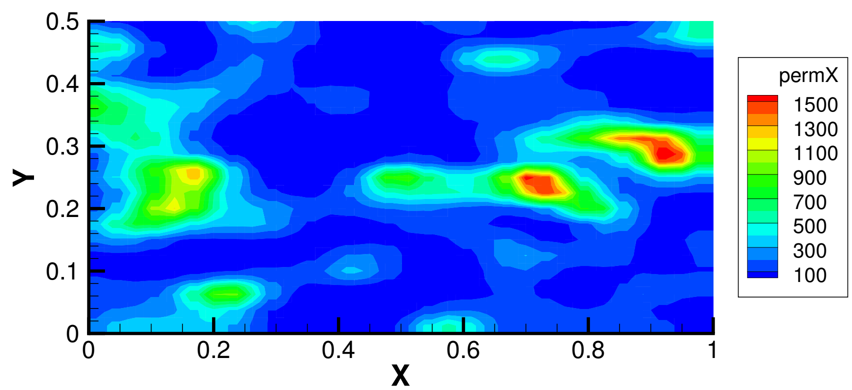

Figure 2: Permeability of the porous medium in the contaminant transport examples.

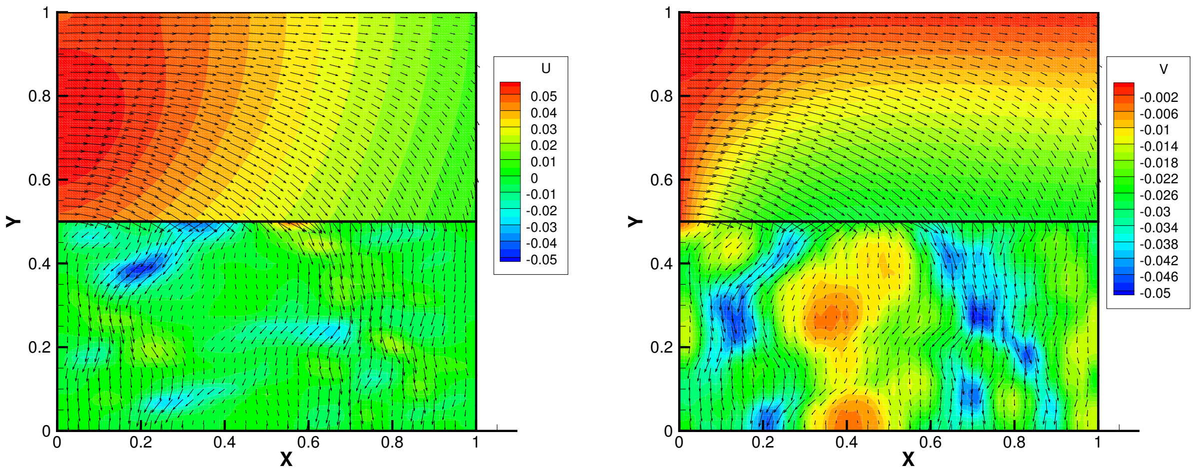

Figure 3: Computed velocity field in the contaminant transport examples. Left: horizontal velocity; right: vertical velocity.

the Darcy region we set no flow on the left and right boundaries and specify pressure on the bottom boundary to simulate a gravity force. The computed velocity field for the two simulations is shown in Figure 3.

In Example 1, a plume of contaminant present at the initial time in the surface water region is transported into the porous media. In Example 2, inflow of contaminant is specified on part of the left boundary in the surface water region. The contaminant front eventually reaches and penetrates into the subsurface water region.

The diffusion tensor is chosen to be $\mathbf{D}_{\Omega_1} = 10^{-6}\mathbf{I}$ in the Stokes region, and

$$\mathbf{D}_{\Omega_2} = \phi d_m \mathbf{I} + d_l |\mathbf{u}| \mathbf{T} + d_t |\mathbf{u}| (\mathbf{I} - \mathbf{T})$$

in the Darcy region, where $\mathbf{T} = \frac{\mathbf{u}\mathbf{u}}{|\mathbf{u}|^2}$ and the parameters values are $\phi = 0.4, d_m = d_l = d_t = 10^{-5}$. Here d_m represents mollecular diffusion, while d_l and d_t represent longitudinal and transverse dispersion, respectively. The simulations were carried out using the forward Euler method for the temporal discretization with $\Delta t = 10^{-3}$ on a square 80×80 mesh.

Due to the discontinuity in the initial (Example 1) or boundary (Example 2) conditions and small diffusion/dispersion values, the simulations exhibit steep concentration gradients. In such cases a slope limiting procedure is often employed in the LDG scheme to remove oscillations [14, 1]. Our approach is based on [24]. For each element local extremum is avoided by comparing the averages of the concentration over the edges with the averages of the concentration over the neighboring elements. The concentration values at the vertices are reconstructed by imposing mass conservation on the element. The procedure is equivalent to an optimization problem with parametrized equality constraints. Tighter constraints introduce more numerical diffusion and lead to a smoother solution. More relaxed constraints allow for better approximation of propagating sharp fronts.

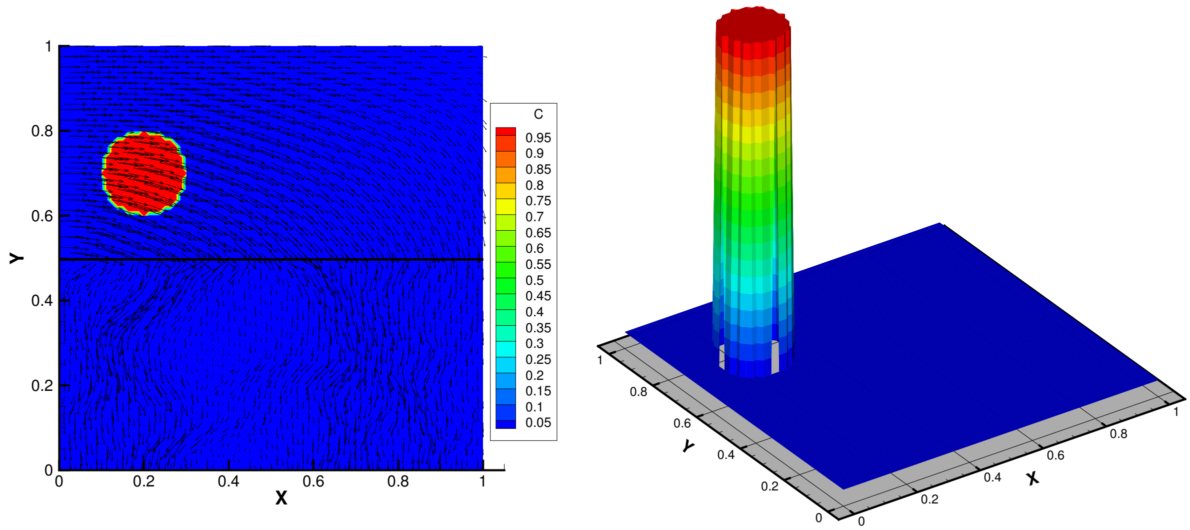

Figure 4: Initial plume, t=0.0. The arrows represent the computed Stokes-Darcy velocity.

Plots of the contaminant concentration at various simulation times are shown in Figures 4–8 for Example 1 and Figures 9–11 for Example 2. Both two and three dimensional views are included for better illustration of the steep concentration gradients.

In Example 1, the plume stays compact while in the surface water region. When it reaches the groundwater region, it starts to spread due to the heterogeneity of the porous media. The discontinuity in the tangential velocity along the interface causes some of the contaminant to lag behind and even move in the opposite direction. Similar behavior is observed in Example 2, where the contaminant front maintains a relatively flat interface in the surface water region and spreads non-uniformly in the porous media. In both cases, the LDG method with slope limiter preserves sharp discontinuities in the concentration without numerical oscillations.

Acknowledgments. This work was partially supported by the NSF grants DMS 0411694 and DMS 0620402 and the DOE grant DE-FG02-04ER25618.

References

[1] V. Aizinger, C. N. Dawson, B. Cockburn, and P. Castillo, *The local discontinuous Galerkin method for contaminant transport*, Advances in Water Resources, 24 (2000), pp. 73–87.

[2] T. Arbogast, M. F. Wheeler, and I. Yotov, *Mixed finite elements for elliptic problems with tensor coefficients as cell-centered finite differences*, SIAM J. Numer. Anal., 34 (1997), pp. 828–852.

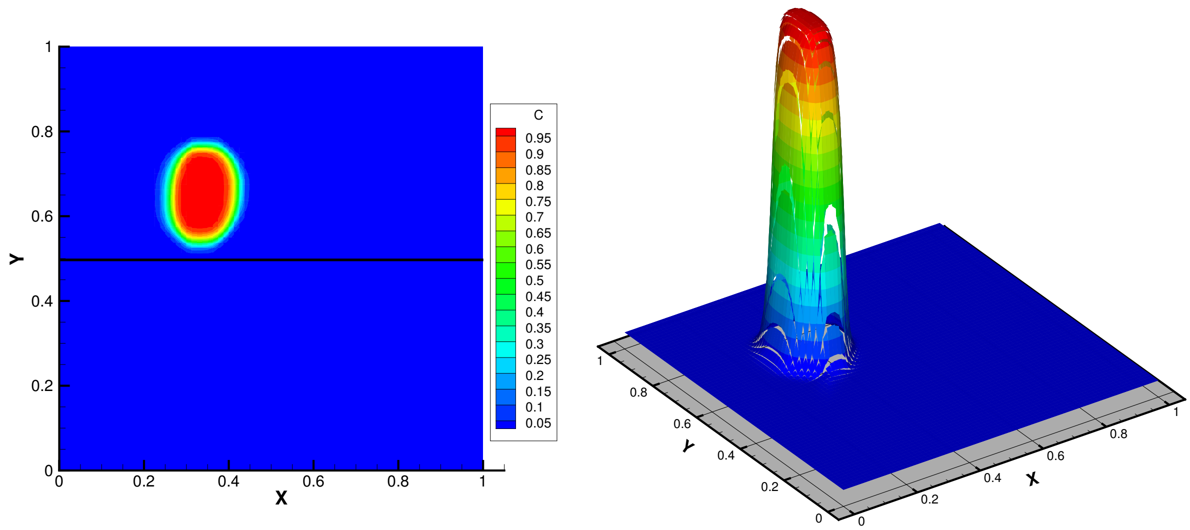

Figure 5: The plume at early time is confined to the surface water region, t=3.0.

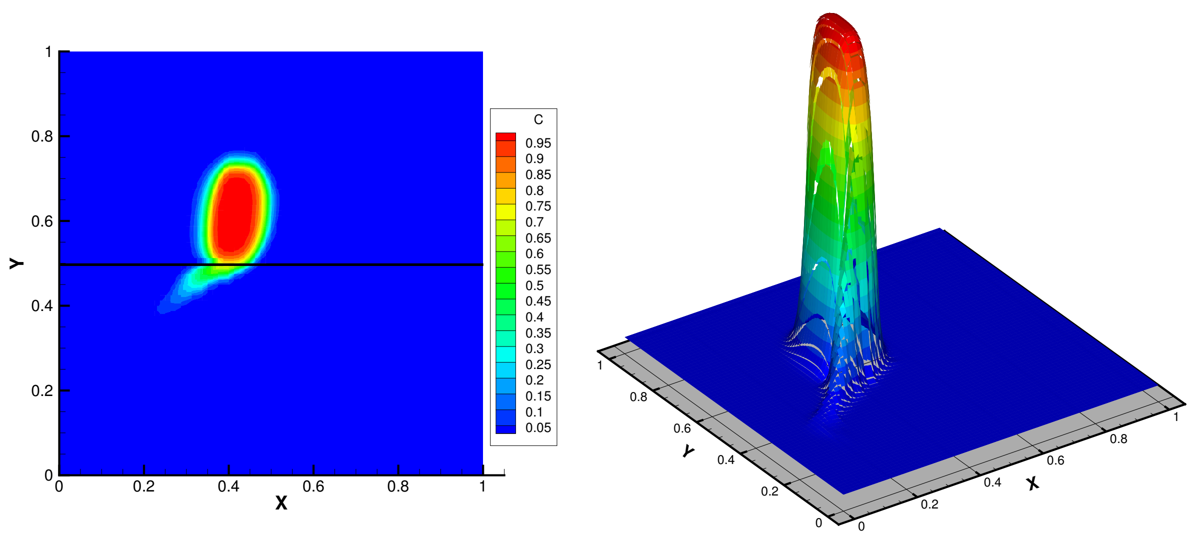

Figure 6: The plume penetrates the porous medium, t=5.0.

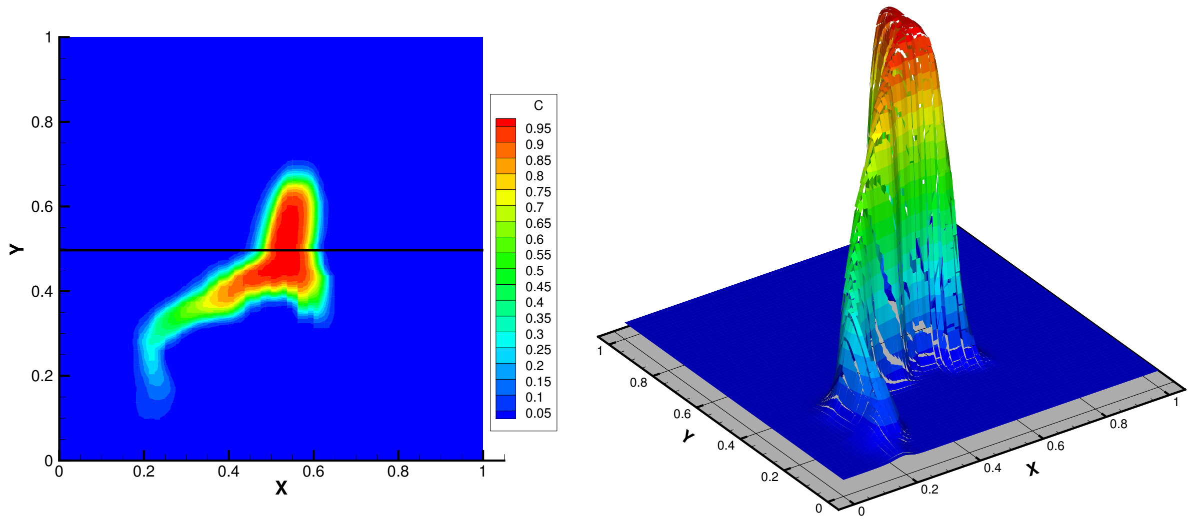

Figure 7: The plume spreads through the porous medium, t=9.0.

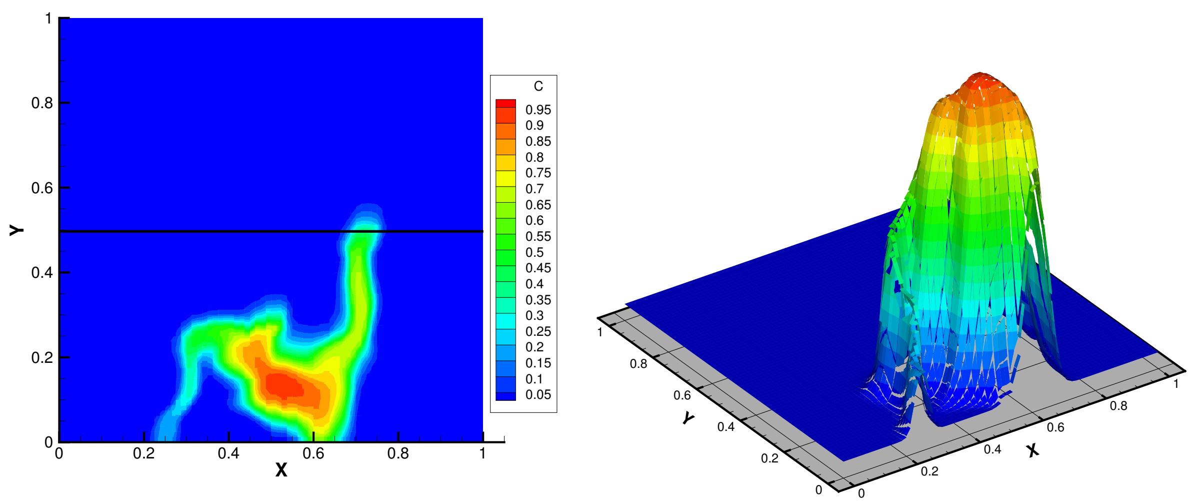

Figure 8: Most of the plume has been transported to the porous medium, t=16.0.

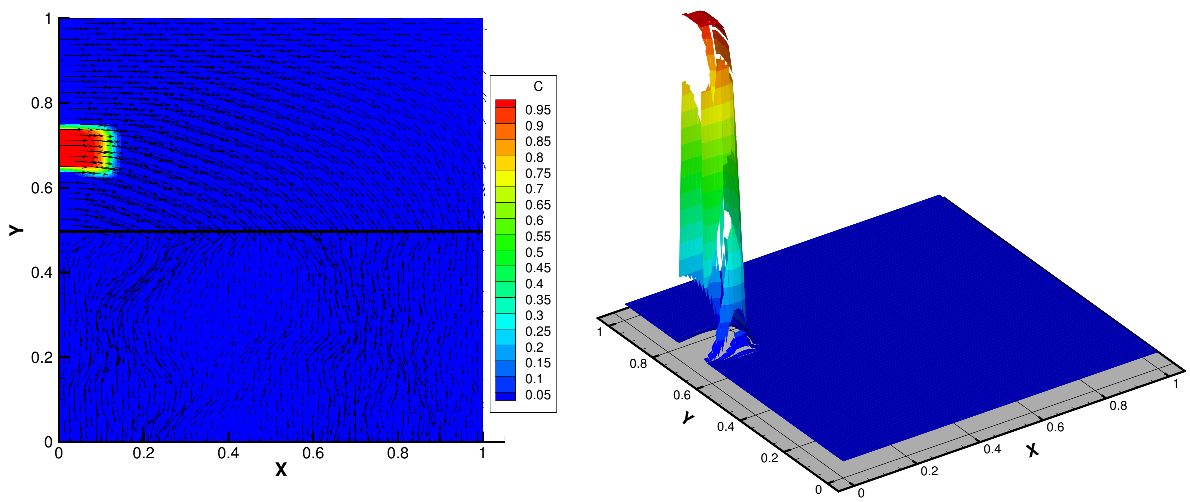

Figure 9: The front enters the surface water region, t=2.0. The arrows represent the computed Stokes-Darcy velocity.

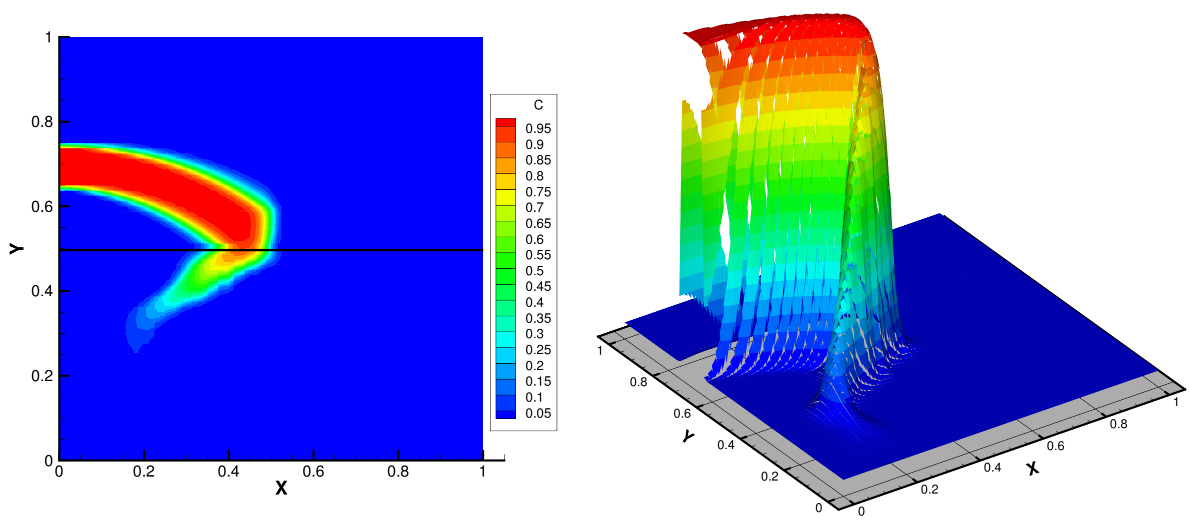

Figure 10: The front reaches the porous medium, t=11.0.

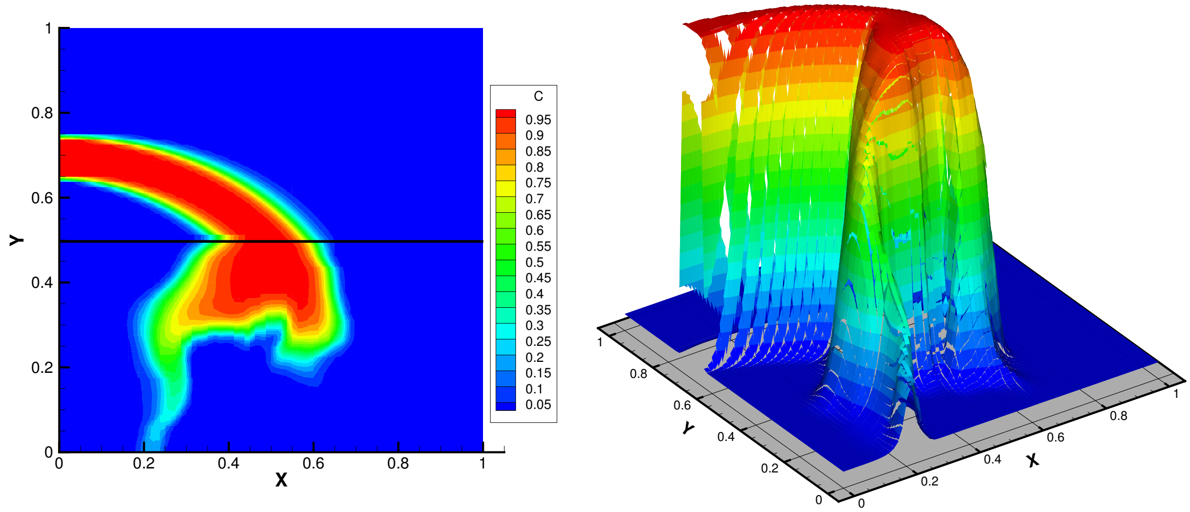

Figure 11: The front propagates inside the porous medium, t=17.0.

[3] D. ARNOLD, *An interior penalty finite element method with discontinuous elements*, SIAM J. Numer. Anal., 19 (1982), pp. 742–760.

[4] D. N. ARNOLD, F. BREZZI, AND M. FORTIN, *A stable finite element for the Stokes equations*, Calcolo, 21 (1984), pp. 337–344 (1985).

[5] G. BEAVERS AND D. JOSEPH, *Boundary conditions at a naturally impermeable wall*, J. Fluid. Mech, 30 (1967), pp. 197–207.

[6] F. BREZZI, J. DOUGLAS, JR., R. DURÀN, AND M. FORTIN, *Mixed finite elements for second order elliptic problems in three variables*, Numer. Math., 51 (1987), pp. 237–250.

[7] F. BREZZI, J. DOUGLAS, JR., M. FORTIN, AND L. D. MARINI, *Efficient rectangular mixed finite elements in two and three space variables*, RAIRO Modèl. Math. Anal. Numèr., 21 (1987), pp. 581–604.

[8] F. BREZZI, J. DOUGLAS, JR., AND L. D. MARINI, *Two families of mixed elements for second order elliptic problems*, Numer. Math., 88 (1985), pp. 217–235.

[9] P. CASTILLO, B. COCKBURN, I. PERUGIA, AND D. SCHÖTZAU, *An a priori error analysis of the local discontinuous Galerkin method for elliptic problems*, SIAM J. Numer. Anal., 38 (2000), pp. 1676–1706 (electronic).

[10] P. CASTILLO, B. COCKBURN, D. SCHÖTZAU, AND C. SCHWAB, *Optimal a priori error estimates for the hp-version of the local discontinuous Galerkin method for convection-diffusion problems*, Math. Comp., 71 (2002), pp. 455–478 (electronic).

[11] Z. CHEN AND J. DOUGLAS, JR., *Prismatic mixed finite elements for second order elliptic problems*, Calcolo, 26 (1989), pp. 135–148.

[12] P. CIARLET, *The finite element method for elliptic problems*, North-Holland, Amsterdam, 1978.

[13] B. COCKBURN AND C. DAWSON, *Some extensions of the local discontinuous Galerkin method for convection-diffusion equations in multidimensions*, in The mathematics of finite elements and applications, X, MAFELAP 1999 (Uxbridge), Elsevier, Oxford, 2000, pp. 225–238.

[14] B. COCKBURN, S. HOU, AND C.-W. SHU, *The Runge-Kutta local projection discontinuous Galerkin finite element method for conservation laws. IV. The multidimensional case*, Math. Comp., 54 (1990), pp. 545–581.

[15] B. COCKBURN AND C.-W. SHU, *The local discontinuous Galerkin method for time-dependent convection-diffusion systems*, SIAM J. Numer. Anal., 35 (1998), pp. 2440–2463.

[16] ——, *Runge-Kutta discontinuous Galerkin methods for convection-dominated problems*, J. Sci. Comput., 16 (2001), pp. 173–261.

[17] M. CROUZEIX AND P.-A. RAVIART, *Conforming and nonconforming finite element methods for solving the stationary Stokes equations. I*, Rev. Française Automat. Informat. Recherche Opérationnelle Sér. Rouge, 7 (1973), pp. 33–75.

[18] C. DAWSON, *Conservative, shock-capturing transport methods with nonconservative velocity approximations*, Comput. Geosci., 3 (1999), pp. 205–227 (2000).

[19] C. DAWSON AND J. PROFT, *A priori error estimates for interior penalty versions of the local discontinuous Galerkin method applied to transport equations*, Numer. Methods Partial Differential Equations, 17 (2001), pp. 545–564.

[20] C. DAWSON, S. SUN, AND M. F. WHEELER, *Compatible algorithms for coupled flow and transport*, Comput. Methods Appl. Mech. Engrg., 193 (2004), pp. 2565–2580.

[21] M. DISCACCIATI, E. MIGLIO, AND A. QUARTERONI, *Mathematical and numerical models for coupling surface and groundwater flows*, Appl. Numer. Math., 43 (2002), pp. 57–74. 19th Dundee Biennial Conference on Numerical Analysis (2001).

[22] R. G. DURÁN AND R. H. NOCHETTO, *Weighted inf-sup condition and pointwise error estimates for the Stokes problem*, Math. Comp., 54 (1990), pp. 63–79.

[23] J. GALVIS AND M. SARKIS, *Non-matching mortar discretization analysis for the coupling Stokes-Darcy equations*, Electron. Trans. Numer. Anal., 26 (2007), pp. 350–384.

[24] H. HOTEIT, P. ACKERER, R. MOSE, J. ERHEL, AND B. PHILIPPE, *New two-dimensional slope limiters for discontinuous Galerkin methods on arbirary meshes*, Int. J. Numer Meth. Engng., 61 (2004), pp. 2566–2593.

[25] W. LAYTON, F. SCHIEWECK, AND I. YOTOV, *Coupling fluid flow with porous media flow*, SIAM J. Numer. Anal., 40 (2003), pp. 2195–2218.

[26] K. A. MARDAL, X.-C. TAI, AND R. WINTHER, *A robust finite element method for Darcy-Stokes flow*, SIAM J. Numer. Anal., 40 (2002), pp. 1605–1631 (electronic).

[27] J. C. NEDELEC, *Mixed finite elements in* $\mathbf{R}^3$, Numer. Math., 35 (1980), pp. 315–341.

[28] R. A. RAVIART AND J. M. THOMAS, *A mixed finite element method for 2nd order elliptic problems*, in Mathematical Aspects of the Finite Element Method, Lecture Notes in Mathematics, vol. 606, Springer-Verlag, New York, 1977, pp. 292–315.

[29] B. RIVIÈRE AND I. YOTOV, *Locally conservative coupling of Stokes and Darcy flows*, SIAM J. Numer. Anal., 42 (2005), pp. 1959–1977.

[30] P. SAFFMAN, *On the boundary condition at the surface of a porous media*, Stud. Appl. Math., L, (1971), pp. 93–101.

[31] S. SUN AND M. F. WHEELER, *Discontinuous Galerkin methods for coupled flow and reactive transport problems*, Appl. Numer. Math., 52 (2005), pp. 273–298.

[32] ——, *Symmetric and nonsymmetric discontinuous Galerkin methods for reactive transport in porous media*, SIAM J. Numer. Anal., 43 (2005), pp. 195–219 (electronic).

[33] C. TAYLOR AND P. HOOD, *A numerical solution of the Navier-Stokes equations using the finite element technique*, Internat. J. Comput. & Fluids, 1 (1973), pp. 73–100.